30796

National Library of Canada | Bibliothèque nationale du Canada

CANADIAN THESES ON MICROFICHE | *THÈSES CANADIENNES SUR MICROFICHE*

NAME OF AUTHOR/*NOM DE L'AUTEUR* BARBARA SHARON PODMORE-PAULSON

TITLE OF THESIS/*TITRE DE LA THÈSE* OPTICAL MODEL ANALYSIS OF P + ^{3}HE ELASTIC SCATTERING

UNIVERSITY/*UNIVERSITÉ* ALBERTA

DEGREE FOR WHICH THESIS WAS PRESENTED/ *GRADE POUR LEQUEL CETTE THÈSE FUT PRÉSENTÉE* MASTER OF SCIENCE

YEAR THIS DEGREE CONFERRED/*ANNÉE D'OBTENTION DE CE GRADE* 1976

NAME OF SUPERVISOR/*NOM DU DIRECTEUR DE THÈSE* Dr. HELMY S. SHERIF

Permission is hereby granted to the NATIONAL LIBRARY OF CANADA to microfilm this thesis and to lend or sell copies of the film.

The author reserves other publication rights, and neither the thesis nor extensive extracts from it may be printed or otherwise reproduced without the author's written permission.

L'autorisation est, par la présente, accordée à la BIBLIOTHÈQUE NATIONALE DU CANADA de microfilmer cette thèse et de prêter ou de vendre des exemplaires du film.

L'auteur se réserve les autres droits de publication; ni la thèse ni de longs extraits de celle-ci ne doivent être imprimés ou autrement reproduits sans l'autorisation écrite de l'auteur.

DATED/*DATÉ* OCTOBER 25, 1976 SIGNED/*SIGNÉ* Barb Paulson

PERMANENT ADDRESS/*RÉSIDENCE FIXÉ* 12811 - 92 Street
Edmonton, Alberta
T5E 3R3

NL-91 (3-74)

INFORMATION TO USERS

THIS DISSERTATION HAS BEEN
MICROFILMED EXACTLY AS RECEIVED

This copy was produced from a microfiche copy of the original document. The quality of the copy is heavily dependent upon the quality of the original thesis submitted for microfilming. Every effort has been made to ensure the highest quality of reproduction possible.

PLEASE NOTE: Some pages may have indistinct print. Filmed as received.

Canadian Theses Division
Cataloguing Branch
National Library of Canada
Ottawa, Canada K1A ON4

AVIS AUX USAGERS

LA THESE A ETE MICROFILMEE
TELLE QUE NOUS L'AVONS RECUE

Cette copie a été faite à partir d'une microfiche du document original. La qualité de la copie dépend grandement de la qualité de la thèse soumise pour le microfilmage. Nous avons tout fait pour assurer une qualité supérieure de reproduction.

NOTA BENE: La qualité d'impression de certaines pages peut laisser à désirer. Microfilmee telle que nous l'avons reçue.

Division des thèses canadiennes
Direction du catalogage
Bibliothèque nationale du Canada
Ottawa, Canada K1A ON4

THE UNIVERSITY OF ALBERTA

OPTICAL MODEL ANALYSIS OF P + ^{3}HE ELASTIC SCATTERING

by

© BARBARA SHARON PODMORE-PAULSON

A THESIS

SUBMITTED TO THE FACULTY OF GRADUATE STUDIES AND RESEARCH IN

PARTIAL FULFILMENT OF THE REQUIREMENTS FOR THE DEGREE OF

MASTER OF SCIENCE

in

NUCLEAR PHYSICS

DEPARTMENT OF PHYSICS

EDMONTON, ALBERTA

FALL, 1976

THE UNIVERSITY OF ALBERTA

FACULTY OF GRADUATE STUDIES AND RESEARCH

The undersigned certify that they have read, and recommend to the Faculty of Graduate Studies and Research, for acceptance, a thesis entitled OPTICAL MODEL ANALYSIS OF P_+ ^{3}HE ELASTIC SCATTERING submitted by Barbara Sharon Paulson in partial fulfillment of the requirements for the degree of Master of Science.

Jack W. Macki
Dr. J.W. Macki

Y. Takahashi
Dr. Y. Takahashi

Douglas M. Sheppard
Dr. D.M. Sheppard
(Co-Supervisor)

Henry S. Sherif
Dr. H.S. Sherif
(Supervisor)

DATE: January 28, 1976

ABSTRACT

The purpose of this work is to investigate further the applicability of the optical model in analysis of very light elastic scattering systems.

The optical model was used to fit the elastic scattering problems: neutron-tritium from 6.0 MeV to 23.0 MeV, and the proton-helium-3 problem from 5.51 MeV to 156 MeV.

The analysis of the data yielded fits to the cross section and polarization data which were usually as good as or better than those obtained by phase shift analysis or the resonating group method. Beyond the use of the standard optical model, exchange terms were added and used in a reanalysis of the p + ^{3}He scattering data. The addition of the exchange terms improved the backward angle fits markedly at 30 MeV and 156 MeV.

It has been shown here that the optical model is a valid method in the analysis of light nuclei scattering and is in many cases easier to use.

ACKNOWLEDGEMENTS

During the course of the three years I took to finish this thesis, I met many people who enriched my life in many ways.

First and foremost is my supervisor, Helmy Sherif, who was so patient and understanding with me and my many distractions. Helmy is not only the best supervisor I could imagine but a very good friend as well. Without his assistance and helpful talks I could never have finished this.

I met a few very special people during this time who have become very close to me: Denise and Orla Aaquist, Peter Johnson, Chris Luursema, and Darryl Hutcheon. They are scattered all over the world now but they have left a lot of themselves with me, and they are with me always.

I have many fond memories of the Nuclear Research staff from discos at 2 a.m. to sleepy summer afternoons filling traps and those a cursed dewers (yech!). Be that as it may, many thanks to the technical and secretarial staff who have helped me in so many ways: Uncle Jock, Auds and John, Greta, Lars, Paul, Cheryl, Little John, ... and leave us not forget those wonderful summer students who plotted graphs for me hour after hour.

I will never forget the professors on staff either: Dr. Roy and his stripped suspenders, Dr. Neilsen who kept me in puzzles, Peter Green, the trivia master, Doc Sheppard and his rotten questions, Dr. Cameron, Dr. MacDonald, Dr. Ken whose computers I continually dumped, Dr. Olsen, . . .

Then there are the other graduate students with whom I passed

the time in pleasant conversation and mad scrambles to finish assignments: Ron Sloboda, my cell mate, Rick Hooper, Bonnie Edwards, Steve MacQuarrie, Tom Neuton, Jan Soukup, Ahmed Hussein, Dave White, Bob McMamis, Steven Seven-Fingers . . .

Now I would like to thank my family who only harassed me a little about how long I was taking to finish and helped me a lot in many little and big ways.

Last but not least I must thank my major distraction: my husband Murray who has made my life as happy as I hoped it would be.

My love to you all!

TABLE OF CONTENTS

Chapter		Page
1	INTRODUCTION	1
2	PHASE SHIFT ANALYSIS	3
3	RESONATING GROUP METHOD	11
	Other Microscopic Calculations	18
4	THEORETICAL DEVELOPMENT OF THE OPTICAL MODEL	29
	Feshbach Theory	31
	Greenlees Theory	35
5	ANALYSIS OF THE EXPERIMENTAL DATA	40
6	EXCHANGE	53
7	DISCUSSION AND CONCLUSION	70
	Discussion	70
	N + ^{3}H	70
	P + ^{3}He	71
	Conclusion	74
REFERENCES		75
BIBILIOGRAPHY		78
APPENDIX: ALTERNATE DERIVATION OF DIFFERENTIAL CROSS SECTION		79

LIST OF TABLES

Table		Page
1	TYPE I PHASE SHIFTS FOR E_p = 30.5 MeV AND FOR E_n = 6 MeV	6
2	RESONANCE PARAMETERS	8
3	PHASE SHIFTS OBTAINED FOR 30.5 MeV P + ^{3}HE ELASTIC SCATTERING BY PHASE SHIFT ANALYSIS (Ha70) AND RESONATING GROUP METHOD (Re71).	22
4	OPTICAL MODEL PARAMETERS	43
5	EXCHANGE PARAMETERS FOR P + ^{3}HE	59

LIST OF FIGURES

Figures Page

1 Phase shift fits to (a) 30.0 MeV differential cross section and (b) 30.5 MeV polarization. 7

2 Phase shift fit to 6 MeV n +^{3}H differential cross section. 9

3 Effective triplet-state p +^{3}He potentials calculated at 6 MeV with the two guassian wave function (solid lines) and the one guassian wave function (dashed lines) for l = 0 to 3. 19

4 Comparison of p +^{3}He differential cross sections calculated using u = 1 and the two guassian wave function (solid lines) (a) and the one guassian wave function (dashed lines) with experimental data at 4.5 MeV, 8.5 MeV and 11.5 MeV (b) with experimental data at 31 MeV. 20

5 Comparison of calculated cross section curves for n +^{3}H scattering with the experimental data points at 19.5 MeV, 21 MeV and 23 MeV. 21

6 Differential cross section (a) and polarization (b) fits for p +^{3}He at 5.51 MeV, 6.82 MeV, 8.82 MeV and 10.77 MeV using microscopic calculation. 27

7 Differential cross section for n +^{3}H at 6 MeV and 14 MeV using microscopic calculation. 28

8 Diagram illustrating vectors used in theoretical derivation. 36

9 Optical model fit to polarization data for n +^{3}H at 22.1 MeV. 44

Figure		Page
10	Optical model fits to differential cross section in $n + {}^3H$ scattering.	45
11	Optical model fit to 5.51 MeV $p + {}^3He$ scattering data.	46
12	Optical model fit to 6.82 MeV $p + {}^3He$ scattering data.	47
13	Optical model fit to 8.82 MeV $p + {}^3He$ scattering data.	48
14	Optical model fit to 10.77 MeV $p + {}^3He$ scattering data.	49
15	Optical model fit to 13.6 MeV $p + {}^3He$ scattering data.	50
16	Optical model fit to 16.2 MeV $p + {}^3He$ scattering data.	51
17	Optical model fit to 49 MeV $p + {}^3He$ scattering data.	52
18	Schematic representation of the $n + \alpha$ scattering problem as a sum of direct and exchange processes. The nucleon-rearrangement process is not shown.	54
19	Optical model fits for $p + {}^3He$ at 30 MeV with and without exchange.	60
20	Optical model fits for $p + {}^3He$ at 156 MeV with and without exchange.	61
21	Optical model fits for $p + {}^3He$ at 19.4 MeV with and without exchange.	62
22	Optical model fits for $p + {}^3He$ at 30 MeV with $C_o = -0.065$ MeV and without exchange.	63
23	Optical model fits for $p + {}^3He$ at 30 MeV with $C_v = -0.4$ MeV and without exchange.	64
24	Optical model fits for $p + {}^3He$ at 30 MeV with $C_{so} = 0.06$ MeV and without exchange.	65
25	Optical model fit for $p + {}^3He$ at 156 MeV with $C_o = -0.075$ MeV.	66

Figure

Page

26 Optical model fit for p + ^{3}He at 156 MeV with C_v = 0.004 MeV. 67

27 Optical model fit for p + ^{3}He at 156 MeV with C_{so} = 0.018 MeV. 68

28 Least squares fit to the V_o's obtained from the optical model fit for p + ^{3}He; yielding the equation: $V_o(E) = 53.75 - 0.869\ E + 0.004\ E^2$. 73

CHAPTER 1

INTRODUCTION

The optical model has generally been thought to apply only to nucleon scattering on medium to heavy nuclei. In heavy nuclei, the energy levels are more closely spaced and therefore, for nucleons with energy $\geq$ 10 MeV, there are no isolated sharp resonances to affect the interaction and the process is describable in terms of a complex potential. Recently, however, several authors (Sa68, De72) have used the optical model to analyze scattering data for very light nuclei with a fair amount of success.

The usual methods of analysis of light nuclei, e.g. ^{3}He, ^{3}H, ^{4}He, are phase shift analyses and resonating group calculations. Phase shift analysis is essentially a phenomenological analysis of data determining the phase shifts for a series of partial waves. This method tends to be cumbersome since a large number of phase shifts and mixing parameters are needed and many extraneous solution sets are found. The optical model is much simpler to use, since once the well geometry is determined, at most five parameters are searched over and in most cases a single solution is found. The resonating group calculations are better in principle since they essentially start from the fundamental two-body interaction. Generally, however, only one channel is considered in the analysis (two channels have recently been used in Mc74 and Ra74) ignoring all other channels. Also, when analyses are made at higher energies, a phenomonological imaginary potential is introduced in order to take into account the effects of the other open channels. Thus, the advantage of the resonating group calculations being microscopic and essentially parameter-free is partially lost. The optical model can be

altered to incorporate most of the effects included in the theoretical calculations. In addition, there is another advantage in using the optical model. In reactions such as (p,n), (p,2p), and (p,pd), the distorted wave Born approximation is used in analysing the data and the optical model parameters are needed in order to determine the distorted waves (Ma74).

The present work consists of the optical model analyses of almost all of the available data for the elastic scattering systems $n + {}^{3}H$ and $p + {}^{3}He$. The resonances that have been "observed" for these systems (T065, To66) are very wide, therefore, it is expected that the model is applicable.

Chapters 2 and 3 are concerned with a brief discussion of phase shift analysis and the resonating group method (and other microscopic calculations), respectively. The theory of the optical model is presented in Chapter 4, followed by the optical model analyses of the $n + {}^{3}H$ and $p + {}^{3}He$ elastic scattering problems in Chapter 5. In Chapter 6, a discussion of exchange effects is given. These are then incorporated within the optical model framework. Chapter 7 entails a discussion of the results of the optical model analysis as compared with those obtained using the other methods of calculation, followed by the concluding comments.

CHAPTER 2

PHASE SHIFT ANALYSIS

One of the most common methods of data analysis for scattering off light nuclei is phase shift analysis. A wave function can be expanded into partial waves. A phase shift is essentially the phase angle through which the scattered partial wave differs from the unscattered one at large distances from the scattering source. Hence, if one knows the phase shifts for all of the partial waves, one can describe the scattering exactly.

As a simple example, one can consider a spin-zero scattering from a spherical potential V(r). Expanding in a series of Legendre polynomials, we have the wave:

$$\psi(r,\theta) = \sum_{\ell} \frac{y_\ell(r)}{r} P_\ell(\cos\theta) \tag{2.1}$$

and the scattering amplitude:

$$f(\theta) = \sum_{\ell} f_\ell P_\ell(\cos\theta) \quad . \tag{2.2}$$

Let

$$k^2 = \frac{2mE}{\hbar^2} \quad , \qquad U(r) = \frac{2mV(r)}{\hbar^2} \tag{2.3}$$

now $y_\ell(r)$ is a regular solution of the radial equation:

$$\left\{\frac{d^2}{dr^2} + \left(k^2 - U(r) - \frac{\ell(\ell+1)}{r^2}\right)\right\} y_\ell(r) = 0 \tag{2.4}$$

and it has the asymptotic form:

$$y_\ell \xrightarrow[r\to\infty]{} a_\ell \sin(kr - \tfrac{1}{2}\ell\pi + \delta_\ell) \tag{2.5}$$

where δ_ℓ is the phase shift and a_ℓ is a normalization constant. We can now write the asymptotic form of ψ as a series of Legendre polynomials:

$$\psi(r,\theta) = e^{i\underset{\sim}{k}\cdot\underset{\sim}{r}} + f(\theta)\frac{e^{ikr}}{r}$$

$$= \sum_\ell \left\{(2\ell+1)i^\ell j_\ell(kr) + f_\ell \frac{e^{ikr}}{r}\right\} P_\ell(\cos\theta) \quad . \tag{2.6}$$

Now, substituting in the asymptotic form of $j_\ell(kr)$ and separating the incoming and outgoing waves, one gets:

$$r\psi(r,\theta) \sim \sum_\ell \left\{(-1)^{\ell+1}\frac{2\ell+1}{2ik} e^{-ikr} + \left(\frac{2\ell+1}{2ik} + f_\ell\right) e^{ikr}\right\} P_\ell(\cos\theta) \quad . \tag{2.7}$$

The asymptotic form of y_ℓ equals the bracketed quantity on the right hand side of Equation (2.7), therefore, one has:

$$a_\ell = i^\ell \frac{2\ell+1}{k} e^{i\delta_\ell} \tag{2.8}$$

and

$$f_\ell = \frac{2\ell+1}{k} e^{i\delta_\ell} \sin\delta_\ell \quad . \tag{2.9}$$

Substituting these into Equation (2.2) one obtains $f(\theta)$ as a function of δ_ℓ:

$$f(\theta) = \frac{1}{k}\sum_{\ell=0}^{\infty} (2\ell+1) e^{i\delta_\ell} \sin\delta_\ell \, P_\ell(\cos\theta) \quad . \tag{2.10}$$

The differential cross section is equal to:

$$\frac{d\sigma}{d\Omega} = |f(\theta)|^2$$

$$= \frac{1}{k^2}\sum_{\ell\ell'} (2\ell+1)(2\ell'+1) e^{i(\delta_\ell - \delta_{\ell'})} \sin\delta_\ell \sin\delta_{\ell'} \, P_\ell(\cos\theta) P_{\ell'}(\cos\theta) \tag{2.11}$$

For an alternate development, refer to Appendix I.

Phase shift analyses have been performed for $p + {}^3He$ elastic scattering for incident proton energies from 1 MeV to 50 MeV (To65, Ha70, Mc70, Ba71). These included the experimental differential cross section data as well as their experimental and extrapolated polarization values in the analyses. Table 1 gives the phase shift values obtained by Harbison et al (Ha70) for the 30 MeV data and the resultant curves are shown in Figure 1. The type 1 solutions are those which use as initial parameters, phase shifts calculated by the resonating group method. This solution set yields s-wave phase shifts which are consistent with those found at very low energies.

An analysis of the $n + {}^3H$ problem was performed by Tombrello (To66) for 6 MeV neutrons. Parameters from the $p + {}^3He$ analysis were used to begin the search. The phase shifts obtained are given in Table 1 and the fit to the differential cross section is shown in Figure 2.

Trombrello also performed single-level analyses for $p + {}^3He$ (To65) and $n + {}^3H$ (To66) problems using a hard core radius of 4.0 fm. The resonance parameters are given in Table 2.

One problem with the phase shift analysis method is that there are upwards of eleven parameters to be searched over, including phase shifts and mixing parameters, even restricting the analysis to $\ell \leq 2$. (The channel-spin-mixing parameters ε account for coupling between singlet and triplet states having the same L and J values such that $\varepsilon_{1,2,3,\ldots}$ $J^\pi = 1^-, 2^+, 3^-$. The tensor couplings of states with the same J^π, but different L values are described by the

TABLE 1

TYPE I PHASE SHIFTS FOR E_p = 30.5 MeV AND FOR E_n = 6 MeV.

	P + ^{3}He SOLUTIONS					N + ^{3}H
δ^j_{sl}	1(A)	1(B)	1(C)	1(D)	1(E)	
δ^0_{00}	-101.5°	-123.0°	-117.5°	-139.0°	-116.0°	-60.7°
δ^1_{10}	-123.0°	-123.0°	-126.5°	-114.0°	-133.0°	-76.2°
δ^1_{01}	69.5°	59.5°	40.0°	36.0°	45.5°	24.9°
δ^0_{11}	31.0°	19.5°	30.0°	33.0°	29.5°	14.3°
δ^1_{11}	30.0°	31.0°	31.5°	31.5°	29.0°	48.9°
δ^2_{11}	30.5°	42.5°	48.5°	55.0°	45.0°	65.1°
$\varepsilon_1(1^-)$	15.5°	30.0°	-13.0°	44.0°	-9.0°	0.0°
δ^2_{02}	1.5°	5.5°	20.5°	11.5°	26.0°	-5.9°
δ^1_{12}	13.5°	-30.0°	-6.0°	0.0°	-9.0°	-
δ^2_{12}	6.0°	3.0°	9.0°	4.5°	3.0°	-
δ_{12}	-	-	-	-	-	-1.4°
δ^3_{12}	12.0°	8.0°	2.0°	6.0°	1.0°	-
$\varepsilon_2(2^+)$	-15.5°	47.0°	6.5°	18.5°	-4.5°	-
δ^3_{03}	7.5°	2.5°	7.5°	5.0°	0.0°	-
δ^2_{13}	-2.0°	1.0°	3.0°	1.0°	1.5°	-
δ^3_{13}	-1.0°	2.0°	-0.5°	2.0°	3.5°	-
δ^4_{13}	7.0°	9.5°	0.0°	7.5°	0.0°	-
$\varepsilon_3(3^-)$	-6.0°	-23.0°	63.0°	-71.5°	-23.5°	-
T_{02}	-3.5°	11.0°	4.5°	-11.5°	-2.5°	-
T_{13}	5.5°	7.5°	-5.5°	-2.5°	-5.5°	-
$\chi^2_{\sigma/n}$	2.69	2.50	2.81	2.54	2.83	0.20
$\chi^2_{p/n}$	0.51	0.57	0.59	0.92	1.06	

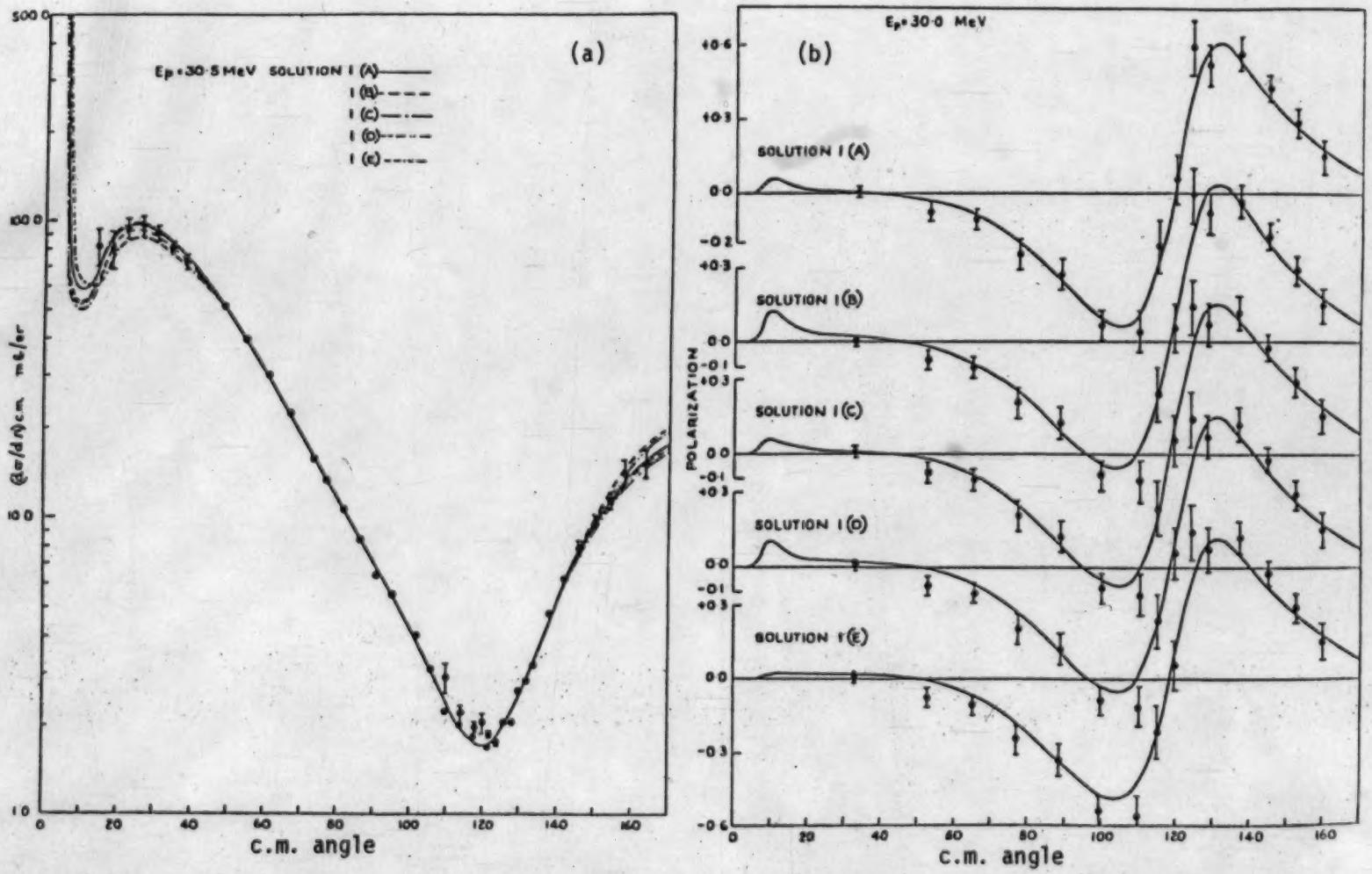

Figure 1 Phase shift fits to (a) 30.0 MeV differential cross section and (b) 30.5 MeV polarization. Reference (Ha70).

TABLE 2

RESONANCE PARAMETERS

SYSTEM	CHANNEL SPIN S	ANGULAR MOMENTUM J^{π}	CENTER OF MASS RESONANCE ENERGY (MeV)	RESONANCE WIDTH γ^2 (MeV)
$p + {}^3He$	1	2^-	47.4	5.5
	1	1^-	6.15	5.5
	1	0^-	7.94	3.3
	0	1^-	9.79	8.8
$n + {}^3H$		2^-	3.4	5.5
		1^-	5.1	5.5

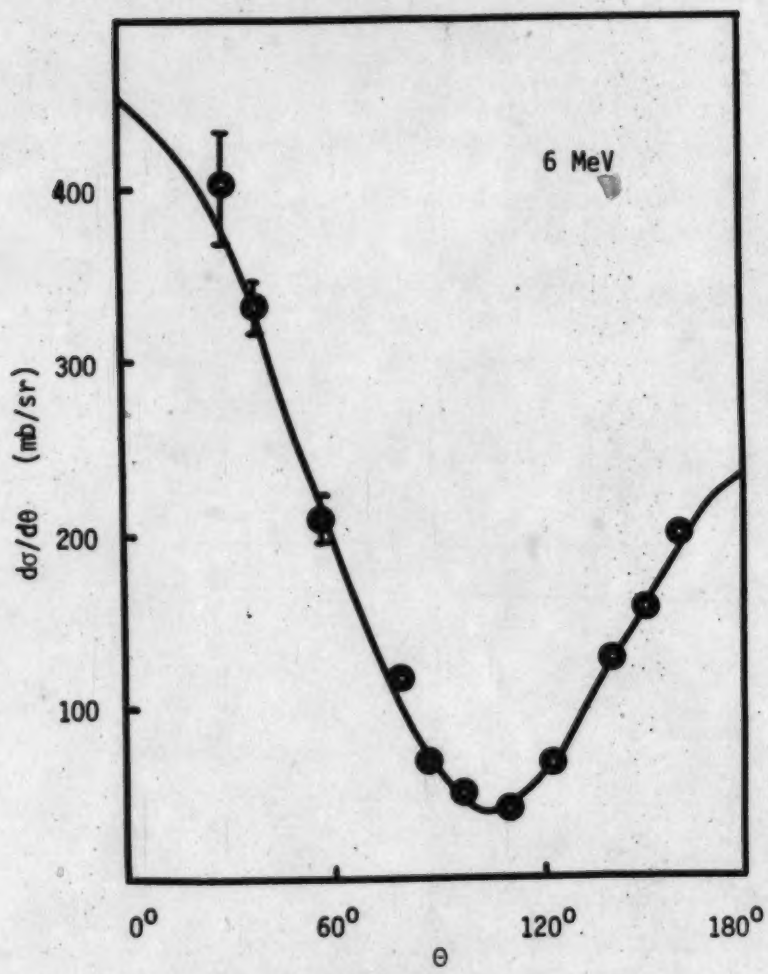

Figure 2 Phase shift fit to 6 MeV n + ^{3}H differential cross section. Reference (To66).

coupling parameters T_{02}, connecting $^3S_1$ and $^3D_1$, and T_{13}, connecting $^3P_2$ and $^3F_2$.)

A major problem is that often many sets of solutions are found which yield equally acceptable fits, for example, there were five type 1 solutions found for the 30 MeV and 49.5 MeV (Ha70) cases. Until further data is available for analysis the extraneous solutions cannot be eliminated. Having several solutions leads to difficulty in extracting reliable physical significance from the resultant phase shifts.

CHAPTER 3

RESONATING GROUP METHOD

The method of resonating group structure has been used to calculate cross sections (polarizations are not done) for scattering systems involving light nuclei. It essentially consists of building a completely antisymmetrized wave function for the whole system, target plus projectile, from channel functions which correspond to the various possible ways of grouping the nucleons, for example, α, ^{3}He, d, etc. (Ta63). This method investigates the close interactions within the nucleus between these groups as opposed to looking at average potentials.

The wave function ψ for a total system of m protons and n neutrons ($m+n=N$) is written as a sum of terms, where each term represents the N nucleons grouped into a particular configuration. Each term is a product of the wave function ϕ describing the motion of the particles within each group, multiplied by a function F^i, depending on the positions and spin variables m_s (total internal angular momentum) of the different groups. The properly antisymmetrized wave function for the whole system, assuming the groups are spinless, has the form:

$$\psi(1,2,\ldots N) = a_1 \sum_{\text{perm}} (\pm 1) \sum_{m^1} F^1 \phi^1_{I,m_I} \phi^1_{II,m_{II}} \cdots$$

$$+ a_2 \sum_{\text{perm}} (\pm 1) \sum_{m^2} F^2 \phi^2_{I,m_I} \cdots + \cdots \qquad (3.1)$$

where $\sum_{\text{perm}} (\pm 1)$ is a summation over all m! permutations of the protons and n! permutations of the neutrons with a change in sign for

odd permutations; the a_i are factors simplifying the normalization; the ϕ^i_{j,m_j} are the different states of the same group and are orthonormal, the m_j singles out the wave function for group j which represents the z component of its angular momentum as m_j; the $\sum_{m^i}$ gives a partial wave function ψ^i corresponding to definite values of the angular momentum of the whole system and its projection along the z-axis.

The main problem is the calculation of the F^i's. They are determined uniquely by demanding that they yield the best wave function ψ, with respect to the variational principle:

$$\delta E = 0 \qquad \text{where} \qquad E = \frac{\int \psi^* \mathcal{H} \psi d\tau}{\int \psi^* \psi d\tau} . \tag{3.2}$$

This yields a set of simultaneous integro-differential equations in the F^i's, which can be transformed into Fredholm integral equations through the use of a generalized Green's function. The condition that the Fredholm determinant for this set of equations vanishes determines the phase shifts, as well as energy levels and transmutation probabilities.

The integro-differential equation is obtained from the Rayleigh-Ritz variational principle in the following way. We have:

$$\delta E = \delta \int \psi^* (H - E) \psi d\tau \tag{3.3}$$

now the wave function is of the form:

$$\psi = \phi(\underset{\sim}{r}) F(\underset{\sim}{R}) \tag{3.4}$$

where ϕ is in internal (relative) coordinates and F is in external (center of mass) coordinates.

Before carrying the treatment any further, let us for simplicity, take the $p + {}^3He$ scattering as an example. To include the exchange of the incident proton and one of the ^3He protons, the wave function must include terms of the form:

$$\phi(1,2,3)F(0,{}^3He) - \phi(0,2,3)F(1,{}^3He) \tag{3.5}$$

where the ^3He contains nucleons 1, 2, 3 and the incident particle is 0; 0, 1, and 2 are protons and 3 is a neutron. The wave function is itself antisymmetrized with respect to the two protons.

Allowing for full exchange the wave function becomes:

$$\psi = \phi(1,2,3)F(0,{}^3He) - \phi(0,2,3)F(1,{}^3He) + \phi(0,1,3)F(2,{}^3He) \ . \tag{3.6}$$

To indicate how the exact calculation is done, a simpler derivation of the integro-differential equation will follow using the simpler wave function of Equation (3.5). For convenience let:

$$\begin{aligned} \phi_1 &\equiv \phi(1,2,3) \qquad & \phi_o &\equiv (0,2,3) \\ F_o &\equiv F(0,{}^3He) \qquad & F_1 &\equiv (1,{}^3He) \end{aligned} \tag{3.7}$$

therefore,

$$\psi = \phi_1 F_o - \phi_o F_1 \ . \tag{3.8}$$

We have the Hamiltonian:

$$H = h_p + h_t + H' + t_p \tag{3.9}$$

where h_p is the internal hamiltonian for the projectile which we

may leave out since it is a single particle; h_t is the internal hamiltonian for the target:

$$h_t = \sum_{i=1}^{3} t_i + \sum_{i<j=1}^{3} v_{ij}$$

such that $h_t\phi = \varepsilon\psi$ (we shall however set $\varepsilon = 0$ for convenience), H' is the interaction hamiltonian between the target and projectile where

$$H' = \sum_{j=1}^{3} v_{pj} \quad ,$$

t_p is the kinetic energy of the relative motion between the projectile and the target:

$$\frac{-\hbar^2}{2m} \nabla^2 \quad ,$$

t_i is the kinetic energy of particle i:

$$\frac{-\hbar^2}{2m} \nabla_i^2$$

and v_{ij} is the interaction between particles i and j.

Therefore, the Hamiltonian may be written:

$$H = \frac{-\hbar^2}{2m} \nabla^2 + V \tag{3.10}$$

where

$$V = \sum_{j} v_{pj} \quad . \tag{3.11}$$

Substituting the above equations into Equation (3.3), one obtains the equation:

$$\delta E = \delta \int (\phi_1 F_o - \phi_o F_1)^* (H - E)(\phi_o F_1 - \phi_1 F_o)^* \, dr_{o\to 3}$$

$$= \delta \int (F_o^* \phi_1^* - F_1^* \phi_o^*) H (\phi_o F_1 - \phi_1 F_o) \, d\tau - E\delta \int (F_o^* \phi_1^* - F_1^* \phi_o^*)(\phi_o F_1 - \phi_1 F_o) \, dr_{o\to 3} \tag{3.12}$$

Since an equation in the external coordinates is required, the variation is performed over F_o^*, therefore,

$$\delta E = \frac{-\hbar^2}{2m}\int[\delta F_o^*\nabla^2 F_o - \delta F_o^*\int\phi_1^*\nabla^2\phi_o F_1] + \int[\delta F_o^* V_D F_o - \delta F_o^*\int\phi_1^* V\phi_o F_1]$$

$$- E\int[\delta F_o^* F_o - \delta F_o^*\int\phi_1^*\phi_o F_1] \qquad (3.13)$$

where

$$V_D = \int\phi_o^* V\phi_o \, dr_{1\to 3}$$

is the average potential over the internal structure. Now, for $\delta E = 0$,

$$\frac{-\hbar^2}{2m}[\delta F_o^*\nabla^2 F_o - \delta F_o^*\int\phi_1^*\nabla^2\phi_o F_1 dr_{1\to 3}] + [\delta F_o^* V_D F_o - \delta F_o^*\int\phi_1^* V\phi_o F_1 dr_{1\to 3}]$$

$$- E[\delta F_o^* F_o - \delta F_o^*\int\phi_1^*\phi_o F_1 dr_{1\to 3}] = 0 \quad . \qquad (3.14)$$

Therefore,

$$[\frac{-\hbar^2}{2m}\nabla^2 + V_D - E]F_o = \int_{r'}\phi_1^*\,(\frac{-\hbar^2}{2m}\nabla^2 + V - E)\phi_o F_1 \, d\tau \quad . \qquad (3.15)$$

Now

$$\int\phi_1^*(\frac{-\hbar^2}{2m} + V - E)\phi_o = K(\underset{\sim}{r},\underset{\sim}{r}') \equiv \text{kernel} \qquad (3.16)$$

where $\underset{\sim}{r}$ is for the unexchanged case and $\underset{\sim}{r}'$ is for the exchanged case. Therefore,

$$[\frac{-\hbar^2}{2m}\nabla^2 + V_D - E]F(\underset{\sim}{r}) = \int K(\underset{\sim}{r},\underset{\sim}{r}')F(\underset{\sim}{r}')d\underset{\sim}{r}' \qquad (3.17)$$

which is the integro-differential equation we are looking for. This equation is not usually used in this form, the functions in Equation (3.17) are expanded in terms of partial waves. We write:

$$\frac{-\hbar^2}{2m}\nabla^2 = \frac{-\hbar^2}{2m}\frac{\partial^2}{\partial r^2} - \frac{\hbar^2}{mr}\frac{\partial}{\partial r} + \frac{\hbar^2 \ell(\ell+1)}{2mr^2} \tag{3.18}$$

$$F(\underset{\sim}{r}) = \sum_{\ell} \frac{f_\ell(r)}{r} P_\ell(\cos\theta) \tag{3.19}$$

and

$$K(\underset{\sim}{r},\underset{\sim}{r'}) = \sum_{\ell,m} \frac{K_\ell(r,r')}{rr'} Y_\ell^{m*}(\Omega) Y_\ell^m(\Omega') \quad . \tag{3.20}$$

Therefore, we can write Equation (3.17) as:

$$\sum_{\ell} \frac{1}{r}\left[\frac{-\hbar^2}{2m}\frac{\partial^2}{\partial r^2} + \frac{\hbar^2\ell(\ell+1)}{2mr^2} + V_D - E\right] f_\ell(r) P_\ell(\cos\theta)$$

$$= \sum_{\ell} \frac{1}{r} \int \sum_{m} \frac{K_\ell(r,r')}{r'r'} Y_\ell^{m*}(\Omega) Y_\ell^m(\Omega') P_\ell(\cos\theta') \quad . \tag{3.21}$$

Equate terms in ℓ and drop the $1/r$, then left multiply both sides by $Y_\ell^{0*}(\Omega)$ and integrate over Ω. Recall that:

$$P_\ell(\cos\theta) = \sqrt{\frac{4\pi}{2\ell+1}}\, Y_\ell^0(\Omega) \tag{3.22}$$

also

$$\int Y_\ell^{m*} Y_{\ell'}^{m'}\, d\Omega = \delta_{\ell\ell'}\delta_{mm'} \tag{3.23}$$

and

$$Y_\ell^{m*}(\Omega) = (-1)^m Y_\ell^{-m}(\Omega) \quad . \tag{3.24}$$

Therefore:

$$\left\{\frac{-\hbar^2}{2m}\frac{\partial^2}{\partial r^2} + \frac{\hbar^2\ell(\ell+1)}{2mr^2} + V_D - E\right\} f_\ell(r) = \int K_\ell(r,r') f_\ell(r')\, dr' \quad . \tag{3.25}$$

Resonating group calculations in the one-channel approximation have been done for $p + {}^3He$ and $n + {}^3H$ elastic scattering systems by Reichstein, Thompson and Tang (Re71). They used two different internal wave functions for the ^3He, a single gaussian and a two gaussian:

$$\phi = \exp[-\tfrac{1}{2}\alpha \sum_{i=1}^{3} (\underset{\sim}{r}_i - \underset{\sim}{R})^2] \tag{3.26}$$

and

$$\phi = \exp[-\tfrac{1}{2}\alpha_1 \sum_{i=1}^{3} (\underset{\sim}{r}_i - \underset{\sim}{R})^2] + c \exp[-\tfrac{1}{2}\alpha_2 \sum_{i=1}^{3} (\underset{\sim}{r}_i - \underset{\sim}{R})^2] \tag{3.27}$$

where the α's are variables, the $\vec{r}_i$ is the position vector of the i^{th} nucleon from the projectile and $\underset{\sim}{R}$ is the position vector of the center of mass of the three nucleon cluster. They used a nucleon-nucleon potential of the form:

$$V_{ij} = [\tfrac{1}{2}(1 + P^{\sigma}_{ij})V_t + \tfrac{1}{2}(1 - P^{\sigma}_{ij})V_s][\tfrac{1}{2}u + \tfrac{1}{2}(2 - u)P^{r}_{ij}] + \frac{e^2}{4r_{ij}}(1 + \tau_{iz})(1 + \tau_{jz}) \tag{3.28}$$

where P^{σ}_{ij} is the spin-exchange operator, P^{r}_{ij} is the space-exchange operator and τ_{iz} is the z-component of the isospin operator for the i^{th} particle. The quantities V_t and V_s are the s-state triplet and singlet potentials given by

$$V_t = - V_{ot}\, e^{-\kappa_t r^2} \tag{3.29}$$

$$V_s = - V_{os}\, e^{-\kappa_s r^2} \tag{3.30}$$

where the constants were found to be (Re71):

$$V_{ot} = 66.92 \text{ MeV} \qquad \kappa_t = 0.415 \text{ fm}^{-2}$$

$$V_{os} = 29.05 \text{ MeV} \qquad \kappa_s = 0.292 \text{ fm}^{-2}$$

and finally, u is an adjustable parameter for best fit.

They found that the two gaussian wave function gave slightly better fits, in general. They also noted that the effective triplet-state $p + {}^3He$ potentials in the odd-ℓ states are quite different from those in the even-ℓ states, see Figure 3. Some of the fits to the experimental $p + {}^3He$ data they found are shown in Figure 4. The $n + {}^3H$ data were analysed in a later paper by Le Mere et al (Le75) and some of their curves are shown in Figure 5. The phase shifts calculated using this method are useful as initial parameters for phase shift analysis (see Chapter 1). The phase shifts obtained by Reichstein et al for 30.5 MeV protons from ^3He are compared in Table 3 with a set obtained by Harbison et al (Ha70).

The resonating group method has several advantages in that it employs a nucleon-nucleon potential, as opposed to a smooth projectile-target average potential. This potential includes exchange terms which have been shown to be important (Re71) and these include the Pauli principle accurately since the wave function is completely antisymmetric. However, due to computational difficulties, approximations are made, such as considering only a single channel, and a relatively simple nucleon-nucleon potential, which cause problems with accuracy, particularly at higher energies. Also, since the nucleon-nucleon potential is purely central, phase shift splitting, channel-spin mixing and polarization cannot be obtained.

OTHER MICROSCOPIC CALCULATIONS

A further refinement to these calculations consists of including all two-body channels, open and closed, in the calculation. Hackenbroich and Heiss have performed such calculations for the

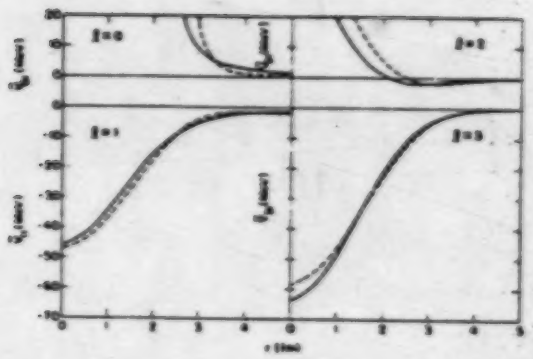

Figure 3 Effective triplet-state p + ^{3}He potentials calculated at 6 MeV with the two guassian wave function (solid lines) and the one guassian wave function (dashed lines) for l = 0 to 3. Reference (Re71).

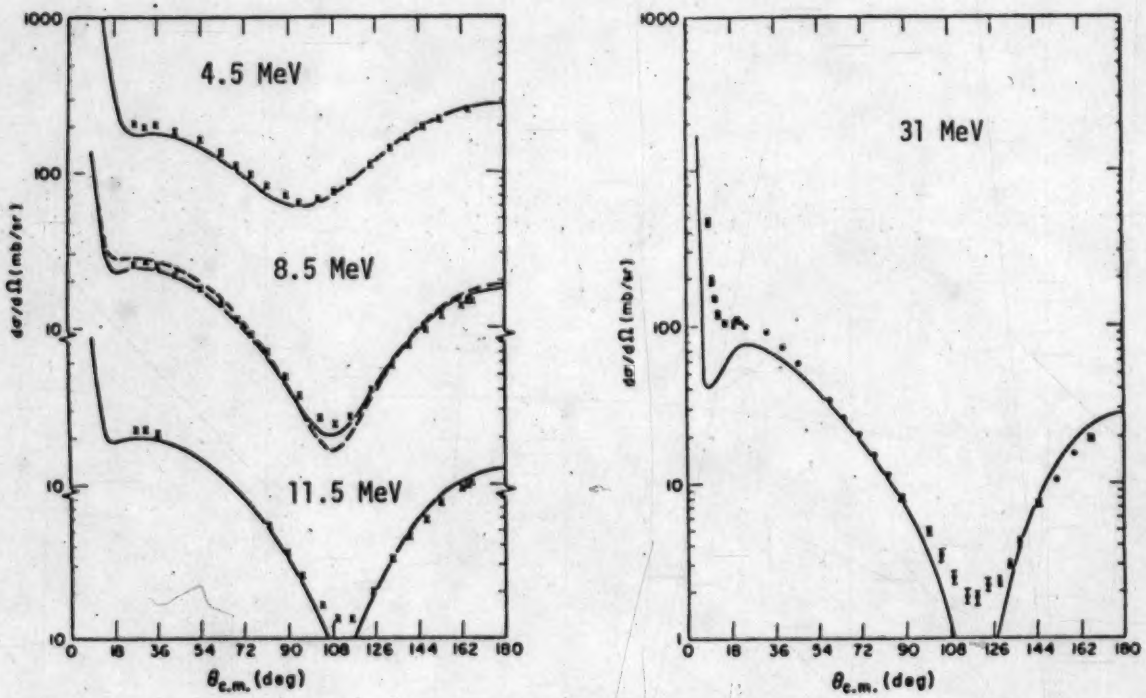

Figure 4 Comparison of p + ^{3}He differential cross sections calculated using u = 1 and the two gaussian wave function (solid lines) (a) and the one guassian wave function (dashed lines) with experimental data at 4.5 MeV, 8.5 MeV and 11.5 MeV (b) with experimental data at 31 MeV. Reference (Re71).

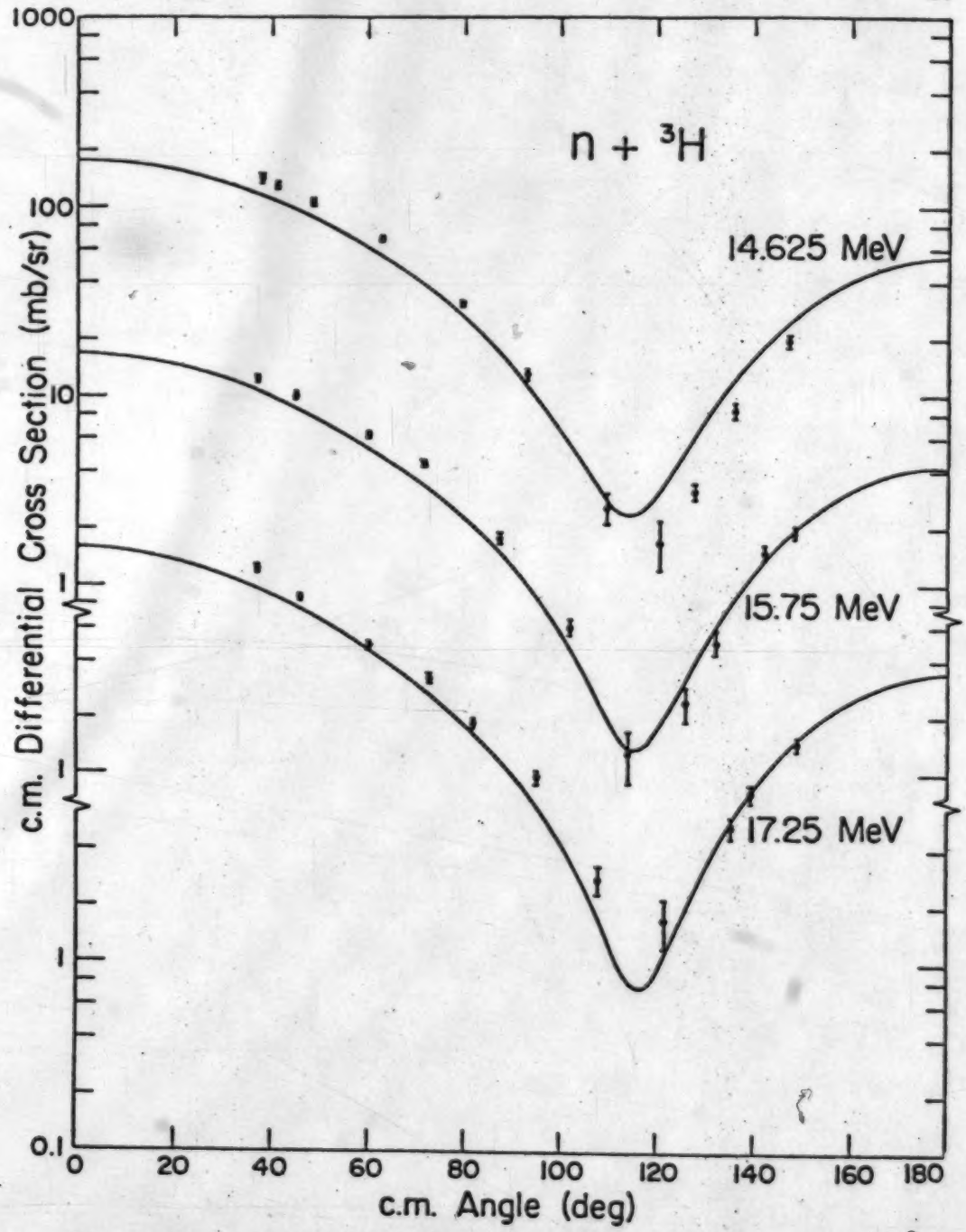

Figure 5 Comparison of calculated cross section curves for n + ^{3}H scattering with the experimental data points at 19.5 MeV 21 MeV and 23 MeV. Reference (Le75).

TABLE 3

Phase shifts obtained for 30.5 MeV p + ^{3}He elastic scattering by phase shift analysis (Ha70) and resonating group method (Re71).

$\delta^j_{s,l}$	PHASE SHIFT RESULT	RESONATING GROUP RESULT
δ^0_{00}	-139.0	-125.4
δ^1_{01}	-114.0	-117.5
δ^1_{10}	36.0	33.6
δ^0_{11}	33.0	
δ^1_{11}	31.5	45.3
δ^2_{11}	55.0	
δ^2_{20}	11.5	1.7
δ^1_{21}	0.0	
δ^2_{21}	4.5	1.9
δ^3_{21}	6.0	
δ^3_{30}	5.0	3.9
δ^2_{31}	1.0	
δ^3_{31}	2.0	4.0
δ^4_{31}	7.5	

$n + {}^3H$ (Ha71) and $p + {}^3He$ (He72) elastic scattering systems.

For each channel included in the calculation, a coupled integro-differential equation comes out of the Rayleigh-Schrodinger variational principle. The resulting set of coupled equations is, in general, unsolvable. Hackenbroich and Heiss devised an approximation which enables them to solve the set of equations (He70). They refer to this method as microscopic calculations.

For n open channels, one gets n linearly independent solutions χ_i^j which satisfy the following boundary conditions:

$$R_i \chi_i^j(R_i) \sim R_i^{L_i+1} \qquad \text{for} \qquad R_i \to 0 \tag{3.31}$$

$$\chi_i^j(R_i) \to \begin{cases} \delta_{ij} f_{L_i}(R_i) + a_i^j g_{L_i}(R_i) & \text{for open channels} \\ 0 & \text{for closed channels} \end{cases} \qquad R_i \to \infty \tag{3.32}$$

They chose a trial wave function of the form:

$$\bar{\chi}_i^j(R_i) = \begin{cases} \delta_{ij} f_L + \bar{a}_i^j \tilde{g}_L + \sum_{\mu=1}^{M} \tilde{\alpha}_{ij}^{\mu} \varphi_{\mu}^j & \text{for open channels} \\ \sum_{\mu=1}^{M} \tilde{\alpha}_{ij}^{\mu} \varphi_{\mu}^j & \text{for closed channels} \end{cases} \tag{3.33}$$

where f_L is a regular coulomb function, g_L is an irregular coulomb function, $\tilde{g}_L$ is a regularized coulomb function and the φ_μ are trial functions of the form:

$$\varphi_\mu^i = R_i^{L_i} \exp(-\beta_\mu R_i^2) \quad . \tag{3.34}$$

The total variational function for boundary condition j, for n-open channels and M trial wave functions, is:

$$\bar{\psi}_j = F_j + \sum_{i=1}^{n} \bar{a}_i^j G_i + \sum_{\lambda=1}^{M} \alpha_\lambda^j \phi_\lambda \tag{3.35}$$

where

$$F_i = \mathcal{A}\{\lambda_i f_{L_i}\} \tag{3.36}$$

$$G_i = \mathcal{A}\{\lambda_i g_{L_i}\} \tag{3.37}$$

$\mathcal{A}$ is the antisymmetry operator and λ_i represents the angular momentum and internal motion of the clusters. The coefficients $\bar{a}^i_j$ are related to the transition matrix elements between the channels i and j (for example, for elastic scattering, we can express the $\bar{a}^i_j$'s in terms of phase shifts.) This function is then used in the Kohn-Hulthéns variational equation:

$$\delta\langle\psi|H - E|\psi\rangle = 0 \ . \tag{3.38}$$

In particular, for the $n + {}^3H$ and $p + {}^3He$, for a given J^π, their ansatz is as follows:

$$\psi = \mathcal{A}\{\sum_\lambda \phi^{J,\pi}_\lambda \chi^{L_\lambda}_\lambda + \sum_\mu \tilde{\phi}^{J,\pi}_\mu \varphi^{L_\mu}_\mu\} \tag{3.39}$$

where ϕ, $\tilde{\phi}$ are the usual surface functions (fixed during the scattering process) and χ_λ and φ_μ are the radial parts of the relative motion functions. For example, for ${}^4Li$:

$$\phi^{J,\pi}_\lambda = \sum_{m_L} C(L_\lambda S_\lambda J, m_L m_S)\rho({}^3He)\xi_{s_\lambda m_S} Y^{m_\lambda}_{L_\lambda}(\Omega) \tag{3.40}$$

and for ${}^4H$:

$$\phi^{J,\pi}_\lambda = \sum_{m_L} C(L_\lambda S_\lambda J, m_L m_S)\rho({}^3H)Y^{m_\lambda}_{L_\lambda}(\Omega) \tag{3.41}$$

where C(...) is a Clebsch-Gordon coefficient, ξ_{sm} is a spin-isospin

function with channel spin S, and ρ is the translationally invariant spatial part of the ^{3}He and ^{3}H wave functions. Now ρ was chosen to be:

$$\rho = \sum_{n=1}^{2} a_n \exp(-b_n \sum_{k>\ell=1}^{3} r_{k\ell}^2) \tag{3.42}$$

where for ^{3}He:

$a_1 = 0.2042$ $\quad$ $b_1 = 0.04$ fm^{-2}

$a_2 = 0.6938$ $\quad$ $b_2 = 0.11$ fm^{-2}

and for ^{3}H:

$a_1 = 0.02$ $\quad$ $b_1 = 0.04$ fm^{-2}

$a_2 = 0.07138$ $\quad$ $b_2 = 0.11$ fm^{-2} .

Heiss and Hackenbroich made a special choice for the central part of the nucleon-nucleon potential, i.e. a local soft core potential composed of a superposition of three gaussians, one repulsive and two attractive (Ei66),

$$V(r) = \sum_{n=1}^{3} a_n \exp(-b_n r^2) \tag{3.43}$$

where a sample set of parameters is:

$a_1 = 880$ MeV $\quad$ $b_1 = 5.40$ fm^{-2}

$a_2 = -70$ MeV $\quad$ $b_2 = 0.64$ fm^{-2}

$a_3 = -21$ MeV $\quad$ $b_3 = 0.48$ fm^{-2}

With these very light nuclei they also use the matrix elements of the simplified potentials with the simplified wave functions (pure s-waves

for A < 5).

The repulsive soft core contained in the central potential necessitated the inclusion of short-range correlations in their wave functions. They chose these to be of the Jastrow type:

$$F = \prod_{m>n} f(|r_m - r_n|) \tag{3.44}$$

where

$$f(r) = 1 - a \exp(-br^2) \tag{3.45}$$

and

$$a = 0.6, \quad b = 3.0 \text{ fm}^{-2} \quad .$$

This was approximated in order to shift the short range correlations to the Hamiltonian FHF $\rightarrow H_{eff}$, since they obtained 2^{12} matrix elements otherwise.

The fits for the $p + {}^3He$ problem are shown in Figure 6 for 8.82 MeV and 10.77 MeV. Both the cross section and polarization fits are excellent, in general, with the cross section fits slightly too small in the backward angles. The differential cross section fits for $n + {}^3H$ at 6.0 MeV and 10.5 MeV are shown in Figure 7 and reproduce the data quite well from above 80° to 180°, being too small in the forward direction.

The microscopic calculations differ from the resonating group calculations in that they assume a form for the wave function and all two-body channels are included specifically.

(a)

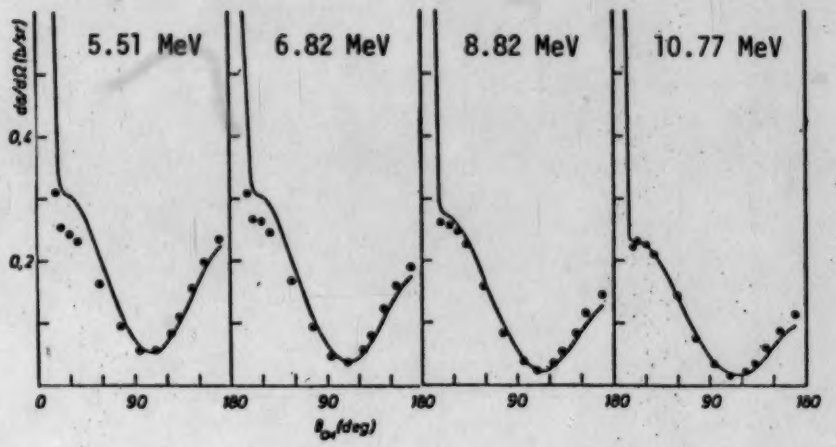

(b)

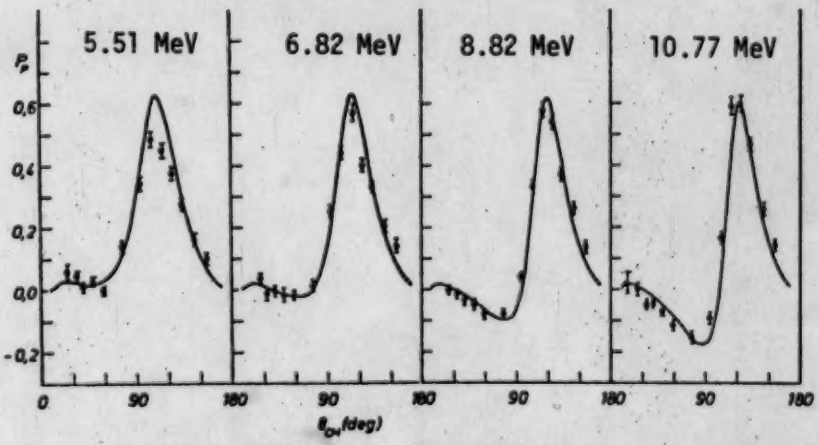

Figure 6 Differential cross section (a) and polarization (b) fits for p +^{3}He at 5.51 MeV, 6.82 MeV, 8.82 MeV and 10.77 MeV using microscopic calculation. Reference (He72).

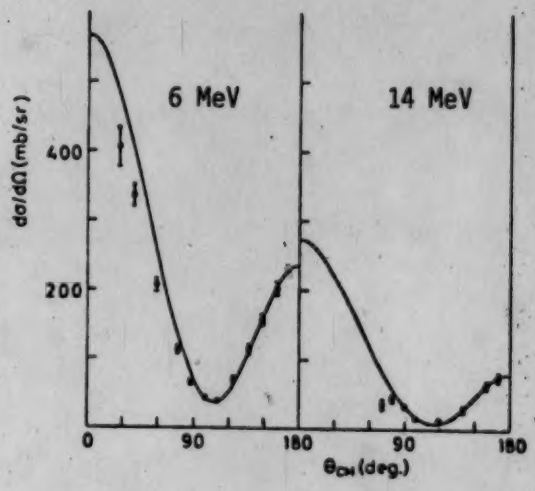

Figure 7 Differential cross section for n + ^{3}H at 6 MeV and 14 MeV using microscopic calculation. Refence (Ha71).

CHAPTER 4

THEORETICAL DEVELOPMENT OF THE OPTICAL MODEL

The semiclassical optical model was first proposed by Serber in 1947 (Se47). This model is referred to as the optical model because of the similarity between the scattering and absorption of particles by a nucleus and the scattering and absorption of light by a cloudy crystal ball.

Consider a wave of wave number

$$k = \sqrt{\frac{2mE}{\hbar^2}} \qquad (4.1)$$

where E is the incident energy and m is the mass of the projectile, incident on a nucleus represented by a complex square well of depth V and radius R. The particle moves more rapidly inside the nucleus due to the attractive nuclear field; it has a new wave number:

$$k + k_1 + \frac{1}{2} iD = \sqrt{\frac{2m(E+V)}{\hbar^2}} \quad . \qquad (4.2)$$

Since the potential V is complex, so is the wave number.

The refractive index of nuclear matter is given by:

$$n = 1 + \frac{k_1}{k} + i\frac{D}{2k} \quad . \qquad (4.3)$$

At high energies, $n \approx 1$ and we can write

$$n^2 \simeq 2(n-1) + 1 \qquad (4.4)$$

since $kR \gg 1$, $k_1 \ll k$ and $D \ll k$, if we let

$$V = U + iW \tag{4.5}$$

then

$$U = v\hbar k_1 \qquad \text{and} \qquad W = \frac{1}{2} v\hbar D \tag{4.6}$$

$$v = \frac{\hbar k}{m} \tag{4.7}$$

where v is the velocity of the incident particle.

Therefore, the nucleon wave function inside the nucleus is:

$$\psi_j = e^{inkz} \tag{4.8}$$

$$= e^{i(k+k_1)z} \; e^{-\frac{1}{2}Dz} \; . \tag{4.9}$$

From Equation (4.6), one can see that the nucleon wave is attenuated by:

$$|\psi_j|^2 = e^{-Dz} \; . \tag{4.10}$$

Using this model, absorption and elastic scattering cross sections for neutrons scattered by a nucleus of radius R, are given by (Ho71):

$$\sigma_A = \pi R^2 \left\{ \frac{1 + [1 - (1+2DR)\exp(-2DR)]}{2D^2R^2} \right\} \tag{4.11}$$

$$\sigma_E = 2\pi \int_0^R |1 - \exp[(-D+2ik_1)S]|^2 \, \rho d\rho \tag{4.12}$$

where

$$S^2 = R^2 - \rho^2 \; . \tag{4.13}$$

Scattering by a complex potential can be treated quantum mechanically as well by allowing the potential in the Schrodinger equation to be complex:

$$V(r) = U(r) + iW(r) \; . \tag{4.14}$$

A complex potential implies that the wave functions $u_L(r)$, where

$$\psi = \sum_L \frac{u_L(r)}{r} P_L(\cos\theta) , \tag{4.15}$$

scattering matrix elements S_L, phase shifts δ_L, and scattering amplitudes $f(\theta)$ are all complex as well.

The Schrodinger equation is of the form

$$\nabla^2\psi + \frac{2m}{h^2}(E - U - iW)\psi = 0 . \tag{4.16}$$

(Note, E is the total real energy of the system, see Equation (4.1).) Multiply Equation (4.16) by ψ^* and subtract ψ times the complex conjugate of (4.16) to obtain:

$$\psi^*\nabla^2\psi - \psi\nabla^2\psi^* = \frac{2imW}{\hbar^2}\psi\psi^* . \tag{4.17}$$

Now, recalling the quantum mechanical expression for particle flux j and density ρ, one sees that Equation (4.17) is equivalent to the classical equation:

$$\frac{\partial\rho}{\partial t} + \text{div } \underset{\sim}{j} = Dv\rho \tag{4.18}$$

where v is the velocity of the projectile inside the nucleus. This is the well known continuity equation with a sink term on the right hand side. Hence, for $W(r) < 0$, the imaginary part of the potential effectively absorbs flux from the beam.

FESHBACH THEORY

Consider the Schrodinger equation

$$E\psi = H\psi \tag{4.19}$$

where $H = H_o + V$, and $H_o(\underset{\sim}{r})$ is the unperturbed nuclear Hamiltonian,

and V is the projectile-target interaction.

The total wave function can be expanded in terms of the scattering states ψ of the projectile and eigenstates ϕ of H_N:

$$\psi(\xi,\underset{\sim}{r}) = \sum_{\lambda} \phi_{\lambda}(\xi)\psi_{\lambda}(\underset{\sim}{r})$$

where ξ are the internal coordinates of the target, and $\underset{\sim}{r}$ is the relative coordinate between the nucleon and the center of mass of the target. Next introduce the projection operators P and Q, where

$$P = 1 - Q \tag{4.20}$$

and P projects out the ground state part of the target wave function. The Schrodinger equation reduces to the coupled equations:

$$(E - H_{PP})P\psi = H_{PQ}Q\psi \tag{4.21}$$

$$(E - H_{QQ})Q\psi = H_{QP}P\psi \tag{4.22}$$

where

$$H_{PQ} = PHQ \text{ , etc .} \tag{4.23}$$

Eliminating $Q\psi$ and applying Equation (4.20), yields an equation for elastic scattering of the projectile:

$$\{E - H_o - \langle\phi_o|V|\phi_o\rangle - \langle\phi_o|VQ(E - H_{QQ})^{-1}QV|\phi_o\rangle\}\ \psi_o = 0 \tag{4.24}$$

where it is assumed that the energy of the nuclear ground state is zero.

Therefore, the generalized optical potential is given by

$$V_{opt} = \langle\phi_o|V|\phi_o\rangle + \langle\phi_o|VQ(E - H_{QQ})^{-1}QV|\phi_o\rangle \tag{4.25}$$

where the second term varies rapidly with energy when E is near an eigenvalue of H_{QQ} giving rise to a resonance in the cross section.

The propagator $(E - H_{QQ})^{-1}$ can be expanded in eigenstates of H_{QQ}, hence, for scattering near an isolated resonance ($E = E_s$), the optical potential is of the form:

$$V_{opt} = \langle\phi_o|V|\phi_o\rangle + \sum_{t\neq s} \frac{\langle\phi_o|VQ|\psi_t\rangle\langle\psi_t|QV|\phi_o\rangle}{E - E_t} + \frac{\langle\phi_o|VQ|\psi_s\rangle\langle\psi_s|QV|\phi_o\rangle}{E - E_s} \tag{4.26}$$

$$= \langle\phi_o|V'|\phi_o\rangle + \frac{\langle\phi_o|VQ|\psi_s\rangle\langle\psi_s|QV|\phi_o\rangle}{E - E_s} \tag{4.27}$$

where V' is chosen such that $\langle\phi_o|V'|\phi_o\rangle$ is equal to the first two terms in the right hand side of Equation (4.26), and its corresponding cross section varies smoothly with energy and includes the effects of distant resonances.

Let ψ_o be the solution to the Schrodinger equation with V' as the potential, and let χ_o be the plane wave solution. From the Gellmann and Goldberger relation, the transition matrix is:

$$T_o = \langle\psi_o|V'|\chi_o\rangle + \langle\psi_o|\frac{W}{1 - GW}|\psi_o\rangle \tag{4.28}$$

where

$$W = \frac{\langle\phi_o|VQ|\phi_s\rangle\langle\phi_s|QV|\phi_o\rangle}{E - E_s} \tag{4.29}$$

and

$$G = (E - T - V')^{-1} \quad . \tag{4.30}$$

Now T can be expressed in Breit-Wigner form:

$$T = T_o + \frac{\langle\psi_o\phi_o|VQ|\phi_s\rangle\langle\phi_s|QV|\phi_o\psi_o\rangle}{E - E_s - \Delta_s + i\frac{\Gamma}{2}} \tag{4.31}$$

where

$$\Delta_s = \langle\phi_s|QV|\phi_o\rangle \frac{P}{E - T - V'} \langle\phi_o|VQ|\phi_s\rangle \tag{4.32}$$

$$\Gamma_s = 2\pi\langle\phi_s|QV|\phi_o\rangle\delta(E - T - V')\langle\phi_o|VQ|\phi_s\rangle \tag{4.33}$$

P is the principle value and T_o is the scattering amplitude due to V' alone and is given by the first term on the right hand side of Equation (4.28).

To derive an optical potential from Equation (4.27), it is necessary to average over the energy using an interval Δ which is large compared to the average resonance spacing. The optical model potential is defined such that its T-matrix corresponds to the energy average of the actual T-matrix. Therefore, average T using a normalized wave function $\rho(E,E')$:

$$\langle T\rangle = \int\rho(E,E')T(E')dE' \quad . \tag{4.34}$$

Choose the Lorentzian form for

$$\rho(E,E') = \frac{I/2\pi}{(E-E')^2 + (I/2)^2} \tag{4.35}$$

where $I \approx 2\Delta/\pi$, and from Cauchy's theorem, we have the relation for the weight function:

$$\int\rho(E,E')F(E')dE' = F(E - \tfrac{i}{2} I) \ . \tag{4.36}$$

Therefore, we have:

$$V(r_o) = V + iW$$

$$V(r_o) = (\phi_o|V'|\phi_o) + \sum_s \frac{(\phi_o|VQ|\phi_s)(\phi_s|QV|\phi_o)}{E - E_s + \frac{1}{2} i I} \qquad (4.37)$$

where r_o is the position of the incident particle.

The imaginary part of the potential is given by:

$$W = -\frac{2}{I} \sum_s \frac{(\phi_o|VQ|\phi_s)(\phi_s|QV|\phi_o)}{1 + 4(E - E_s)^2/I^2} \quad . \qquad (4.38)$$

Now the denominator damps contributions from all levels such that $|E - E_s| \gg I/2$, therefore:

$$W \approx -\frac{\pi}{\Delta} \sum_{s=1}^{N} (\phi_o|VQ|\phi_s)(\phi_s|QV|\phi_o) \quad . \qquad (4.39)$$

In practice, however, this expression is difficult to evaluate.

GREENLEES THEORY

The interaction between the target and the projectile is the sum of all the projectile-nucleon-target-nucleon interactions $v(|\underset{\sim}{r} - \underset{\sim}{r}'|)$ (See Figure 8).

Look at the first term in Equation (4.26):

$$V_{opt} \equiv \langle\phi_o|V|\phi_o\rangle \qquad (4.40)$$

now,

$$V = \sum_{i=1}^{A} v(\underset{\sim}{r} - \underset{\sim}{r}') \qquad (4.41)$$

therefore,

$$V_{opt} = \langle\phi_o| \sum_{i=1}^{A} v(\underset{\sim}{r} - \underset{\sim}{r}')|\phi_o\rangle \qquad (4.42)$$

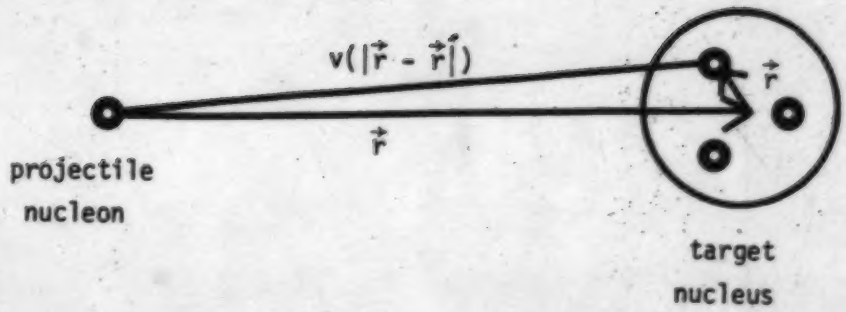

Figure 8 Diagram illustrating vectors used in theoretical derivation.

or

$$V(\underset{\sim}{r}) = \int \rho_m(\underset{\sim}{r}')v(|\underset{\sim}{r} - \underset{\sim}{r}'|)d\underset{\sim}{r}' \tag{4.43}$$

where $\rho_m(\underset{\sim}{r}')$ is the density distribution of nuclear matter. Now, V(r) is the first term in the Feshbach expansion. Greenlees et al (Gr68, Gr70a, Gr70b) ignored all the correction terms and used Equation (4.43) as their potential. This treatment leads only to the real parts of the optical potential. They then used the following form for the nucleon-nucleon interaction:

$$\begin{aligned} V(|\underset{\sim}{r}_i - \underset{\sim}{r}_j|) \equiv V(\underset{\sim}{r}) \\ = V_D(\underset{\sim}{r}) + V_\tau(\underset{\sim}{r})\tau_i\cdot\tau_j + V_\sigma(\underset{\sim}{r})\sigma_i\cdot\sigma_j + V_{\sigma\tau}(\underset{\sim}{r})(\sigma_i\cdot\sigma_j)(\tau_i\cdot\tau_j) \\ + [V_t(\underset{\sim}{r}) + V_{t\tau}(\underset{\sim}{r})\tau_i\cdot\tau_j]S_{ij} \\ + \frac{1}{\hbar} V_s(\underset{\sim}{r})[(\underset{\sim}{r}_i - \underset{\sim}{r}_j)\times(\underset{\sim}{p}_i - \underset{\sim}{p}_j)\cdot(\sigma_i + \sigma_j)\ ] \end{aligned} \tag{4.44}$$

where S_{ij} is the tensor force operator and

$$S_{ij} = 3(\sigma_i\cdot\hat{r})(\sigma_j\cdot\hat{r}) - \sigma_i\cdot\sigma_j \tag{4.45}$$

also: σ's are the Pauli spin operators, τ's are the isospin operators, and $\underset{\sim}{P}$ refers to the particle momentum operator. For nuclei of spin zero, one can write the potential in the form:

$$V(\underset{\sim}{r}) = V_R(\underset{\sim}{r}) + V_I(\underset{\sim}{r}) + V_S(\underset{\sim}{r}) \tag{4.46}$$

where V_R is purely central, and V_I and V_S contain spin and isospin terms.

To find expressions for these potentials, breakdown the nuclear matter density into its proton and neutron components:

$$\rho_m(\underset{\sim}{r}) = \rho_p(\underset{\sim}{r}) + \rho_n(\underset{\sim}{r}) \quad . \tag{4.47}$$

Assume spherical distributions and substitute Equations (4.44) and (4.47) into Equation (4.43). This gives us:

$$V_R(r) = \int \rho_m(\underset{\sim}{r}')V_D(|\underset{\sim}{r}-\underset{\sim}{r}'|)d\underset{\sim}{r}' \tag{4.48}$$

$$V_I(r) = \tau_z \int [\rho_p(\underset{\sim}{r}') - \rho_n(\underset{\sim}{r}')]V_\tau(|\underset{\sim}{r}-\underset{\sim}{r}'|)d\underset{\sim}{r}' \tag{4.49}$$

$$V_S(r) = -\left\{\frac{1}{\hbar}\sum_{n=1}^{\infty}\frac{4\pi}{(2n+1)!}\frac{2n}{r}\frac{d}{dr}\left\{\frac{2(n+1)}{r}\frac{d^{2n-3}}{dr^{2n-3}}\rho_m(r) + \frac{d^{2n-2}}{dr^{2n-2}}\rho_m(r)\right\}\int_0^{\infty} u_{LS}(\eta)\eta^{2n+2}d\eta\right\}\underset{\sim}{L}\cdot\underset{\sim}{\sigma} \quad . \tag{4.50}$$

Under 50 MeV, it is a good approximation to use only the first term for V_S which gives:

$$V_S(r) = -\frac{1}{\hbar}\frac{4\pi}{3}\frac{1}{r}\frac{d}{dr}\rho_m(r)\int V_S(\eta)\eta^4 d\eta\, \underset{\sim}{L}\cdot\underset{\sim}{\sigma} \quad . \tag{4.51}$$

Forms for the nuclear distributions and the radial functions are needed to perform calculations. These are usually chosen as follows:

$$\rho_m(r) = \rho_m(0)/1 + \exp\left(\frac{r - R_m}{a_m}\right) \tag{4.52}$$

$$V_D(r) = V_D\frac{e^{-\mu r}}{r} \tag{4.53}$$

where V_D and μ are adjustable. Also assume:

$$\rho_p(r) = \frac{Z}{A}\,\rho_m(r) \tag{4.54}$$

$$\rho_n(r) = \frac{N}{A}\,\rho_m(r) \tag{4.55}$$

$$V_I(r) = \zeta\,\frac{N-Z}{A}\;\tau_Z\,V_R(r) \tag{4.56}$$

if

$$V_\tau(r) = \zeta V_D(r)$$

and $$\tau_Z = \begin{cases} +1 & \text{for neutrons} \\ -1 & \text{for protons} \end{cases}$$

In their analysis of 30 MeV proton scattering experiments by a range of nuclei, Greenlees et al (Gr68) used r_m, a_m, V_R, W_D, W_V, r_w and a_w as variable parameters and obtained fits to the data as successful as those obtained by other methods.

CHAPTER 5

ANALYSIS OF THE EXPERIMENTAL DATA

Optical model analyses of elastic scattering by light nuclei have been performed in the past with varying degrees of success. The potentials used were generally of the form:

$$U(r) = -V_o f(r,R_o,a_o) - iW_v f(r,R_i,a_i) + 4ia_i W_D \frac{d}{dr} f(r,R_i,a_i) + \left(\frac{\hbar}{m_\pi c}\right)^2 \frac{1}{r}\frac{d}{dr} f(r,R_{so},a_{so})\underset{\sim}{\sigma}\cdot\underset{\sim}{L} \qquad (5.1)$$

where

$$f(r,R_x,a_x) = \left\{1 + \exp\left(\frac{r-R_x}{a_x}\right)\right\}^{-1} \qquad (5.2)$$

and

$$R_x = r_x A^{1/3} \qquad (5.3)$$

In 1964, Kim et al (Ki64) analysed the differential cross section of $p + {}^3He$ at 31 MeV without much success. In their potential they chose $R_o = R_i = R_{so}$, and a surface peaked gaussian was used instead of the Woods-Saxon derivative. In 1968, $n + {}^4He$ and $p + {}^4He$ data were analysed by Satchler et al (Sa68) for energies from 0.3 MeV to 18 MeV, and fits were obtained which closely reproduced the experimental data. The energies considered were below the threshold energy for ^4He breakup, therefore, there were no imaginary terms in the potential. In 1970, Thompson et al (Th70) analysed $p + {}^4He$ at energies between 31 MeV and 55 MeV successfully. Recently, Devries et al (De72) analysed $p + d$ using a spin independent optical potential but they had to include exchange effects to obtain good fits. They also

attempted to fit the n+ ^{3}H 18 MeV cross section data.

In the present analysis of the n+ ^{3}H and p+ ^{3}He elastic scattering data, an optical model of the above form is used. The parameters were obtained using the search code SNOOPY (Sc69) and were refined with the double precision code TASHTASH (Shpc). The final parameters were determined generally by minimum values for chi-squared values:

$$\chi^2 = \frac{\chi^2_\sigma}{N_\sigma} + \frac{\chi^2_p}{N_p} \qquad (5.4)$$

where N_σ and N_p are the numbers of data points for differential cross section and polarization, also:

$$\chi^2_\sigma = \sum_{i=1}^{N_\sigma} \left[\frac{\sigma_{ex}(\theta_i) - \sigma_{th}(\theta_i)}{\Delta\sigma_{ex}(\theta_i)} \right]^2 \qquad (5.5)$$

and $\sigma_{ex}(\theta_i)$, $\sigma_{th}(\theta_i)$, and $\Delta\sigma_{ex}(\theta_i)$ are the experimental, theoretical and experimental error values of the cross section at a center of mass angle θ_i, similarly for χ^2_p.

The analysis was begun with the n+ ^{3}H problem (Sh72). The polarization data at 22.1 MeV was analysed first using initial parameters from Devries et al (De72) and estimated values for the spin-orbit parameters. The well geometry was determined and then fixed for ALL further calculations. Next, the well parameters were determined and used as the initial values for the neighbouring energies. All available data was analysed. In the p+ ^{3}He (Po74) analysis, the searches were started at 19.4 MeV. In this part of the analysis, due to the large amount of available data, only

energies for which both differential cross section and polarization data were available were included in the analysis. This is important since the best differential cross section and polarization fits do not always have compatible parameters. The optical model parameters resulting from these analyses are given in Table 4. The corresponding best fit curves are shown in Figures 9 through 17. The curves for $p + {}^{3}He$ at 19.4 MeV, 30 MeV, and 156 MeV will be presented in Chapter 6.

The curves on the whole fit the experimental data quite well. The differential cross section fits are generally too small in the backward angles. The polarization fits are excellent with the single exception of the $p + {}^{3}He$ curve at 49 MeV. It is noted that the 49 MeV $p + {}^{3}He$ data was extremely difficult to fit using reasonable parameters.

TABLE 4

OPTICAL MODEL PARAMETERS

r_o = 1.488 fm r_i = 1.501 fm r_{so} = 1.049 fm r_c = 1.3 fm

a_o = 0.144 fm a_i = 0.378 fm a_{so} = 0.289 fm

E_n (MeV)	V_o (MeV)	W_v (MeV)	W_D (MeV)	V_{so} (MeV)	χ^2_σ/N_σ	χ^2_p/N_p
for n + ^{3}H						
6.0	50.35	0.52	0.0	1.73	1.7	-
9.0	47.36	1.49	0.0	2.47	6.8	-
18.0	42.98	4.69	0.0	3.22	2.2	-
19.5	42.07	5.46	0.0	3.07	2.1	-
21.0	42.0	6.19	0.0	3.77	5.9	-
22.1	41.60	7.63	0.0	5.94	-	1.3
23.0	41.86	7.38	0.0	5.24	3.6	-
for p + ^{3}He						
5.51	49.7	0.0	0.0	0.72	107.5	7.4
6.82	48.26	0.0	0.0	0.86	156.7	13.0
8.82	46.1	1.2	0.0	1.31	18.6	8.1
10.77	44.2	1.37	0.0	1.43	22.6	8.7
13.6	41.63	1.18	0.0	1.47	304.7	40.2
16.2	38.7	0.94	0.0	1.6	324.9	45.3
19.4	38.2	3.6	0.0	3.2	303.1	248.8
30.0	32.2	6.05	0.0	7.34	34.6	7.3
49.0	17.44	12.64	0.0	12.64	138.3	20.1
156.0	9.86	8.61	0.0	4.26	275.4	20.3

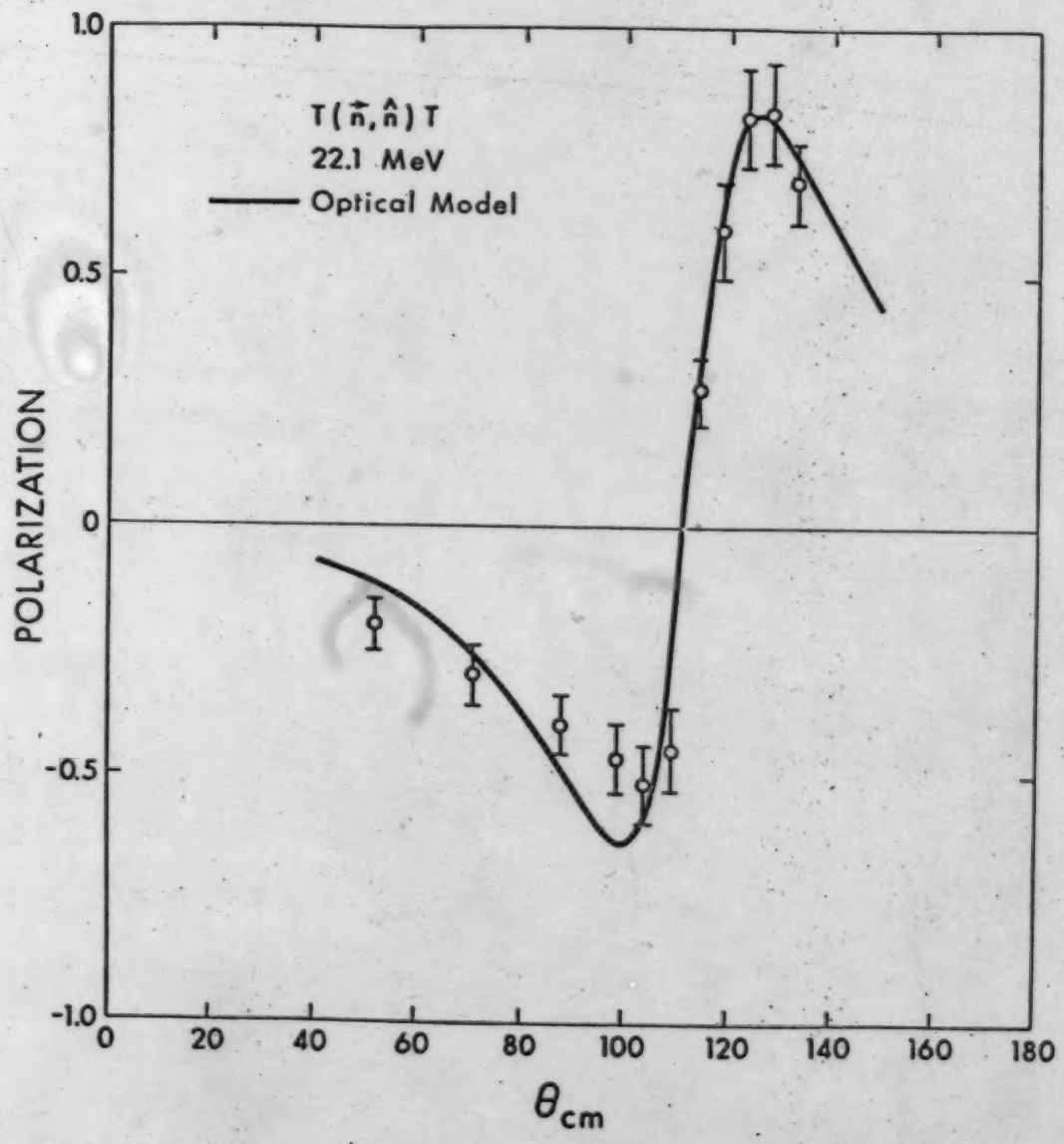

Figure 9 Optical model fit to polarization data for n + ^{3}H at 22.1 MeV. Data (Se72).

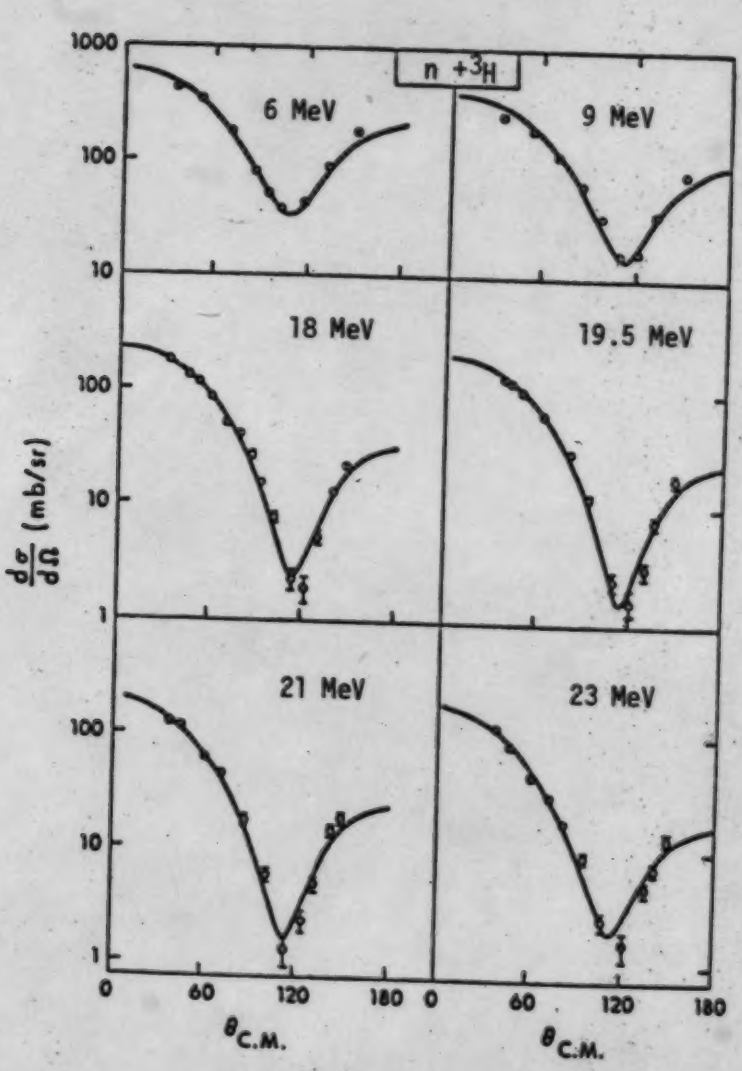

Figure 10 Optical model fits to differential cross section in n +^{3}H scattering. Data (Se72).

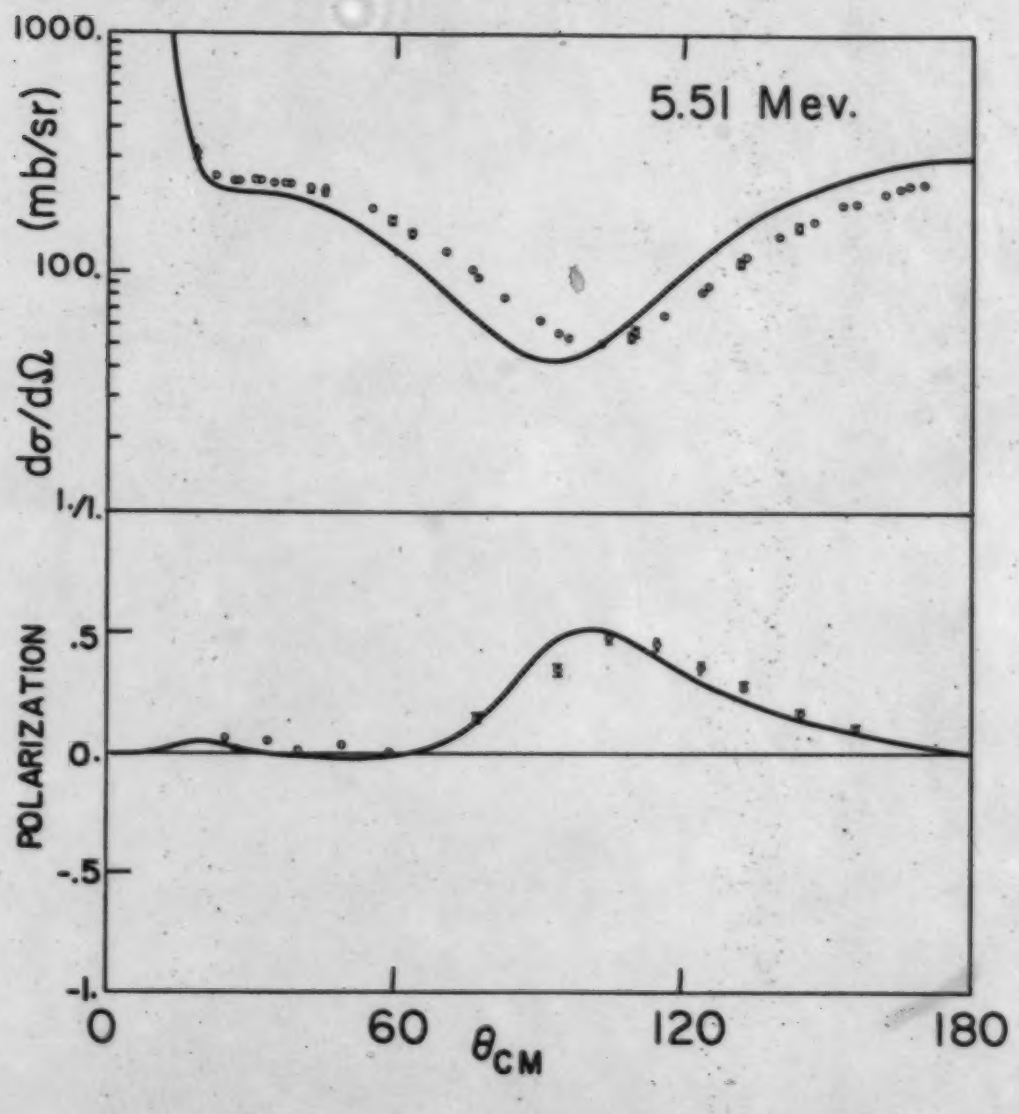

Figure 11 Optical model fit to 5.51 MeV p + ^{3}He scattering data (Mc64, C164, Mo69).

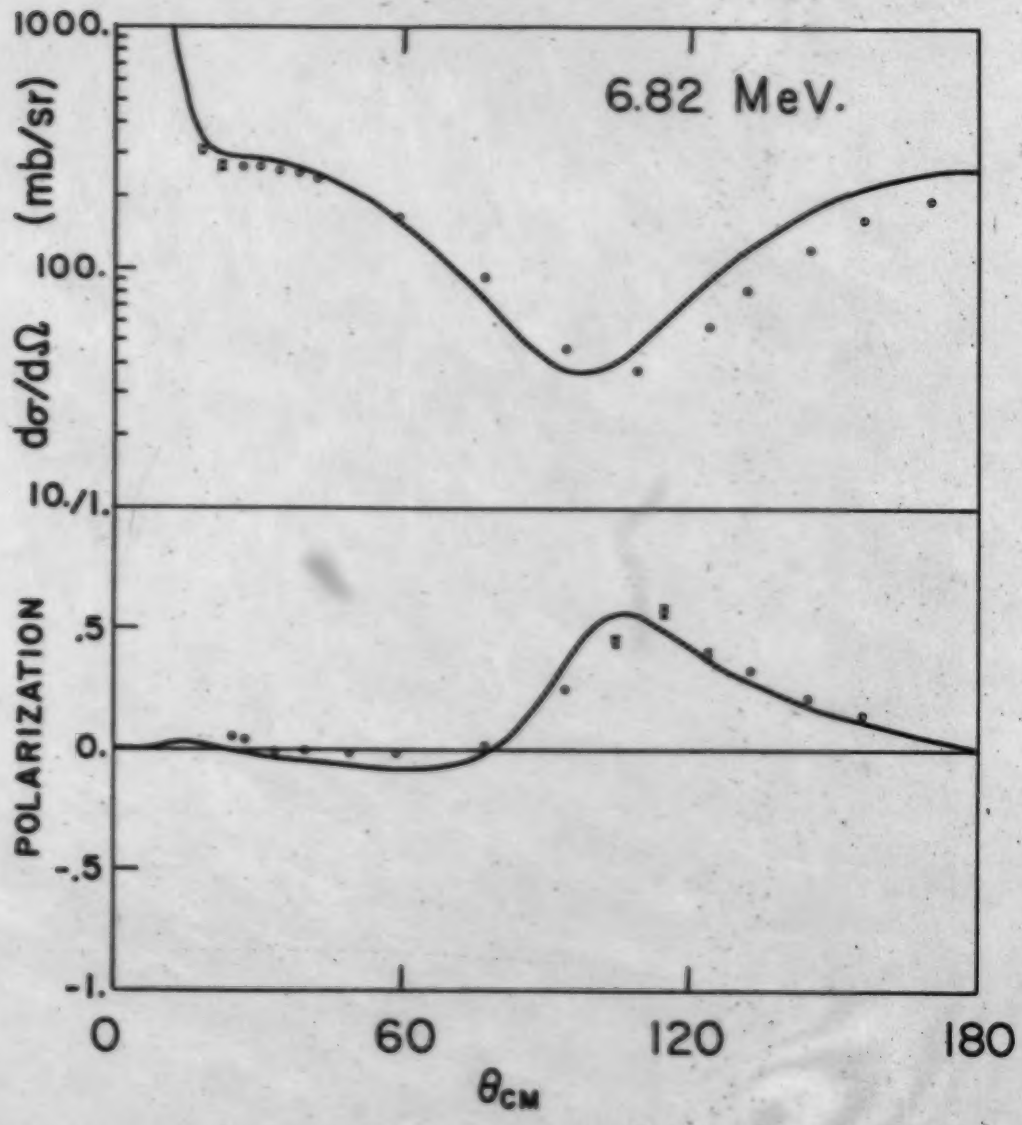

Figure 12 Optical model fit to 6.82 MeV p + ^{3}He scattering data (Mc64, M069).

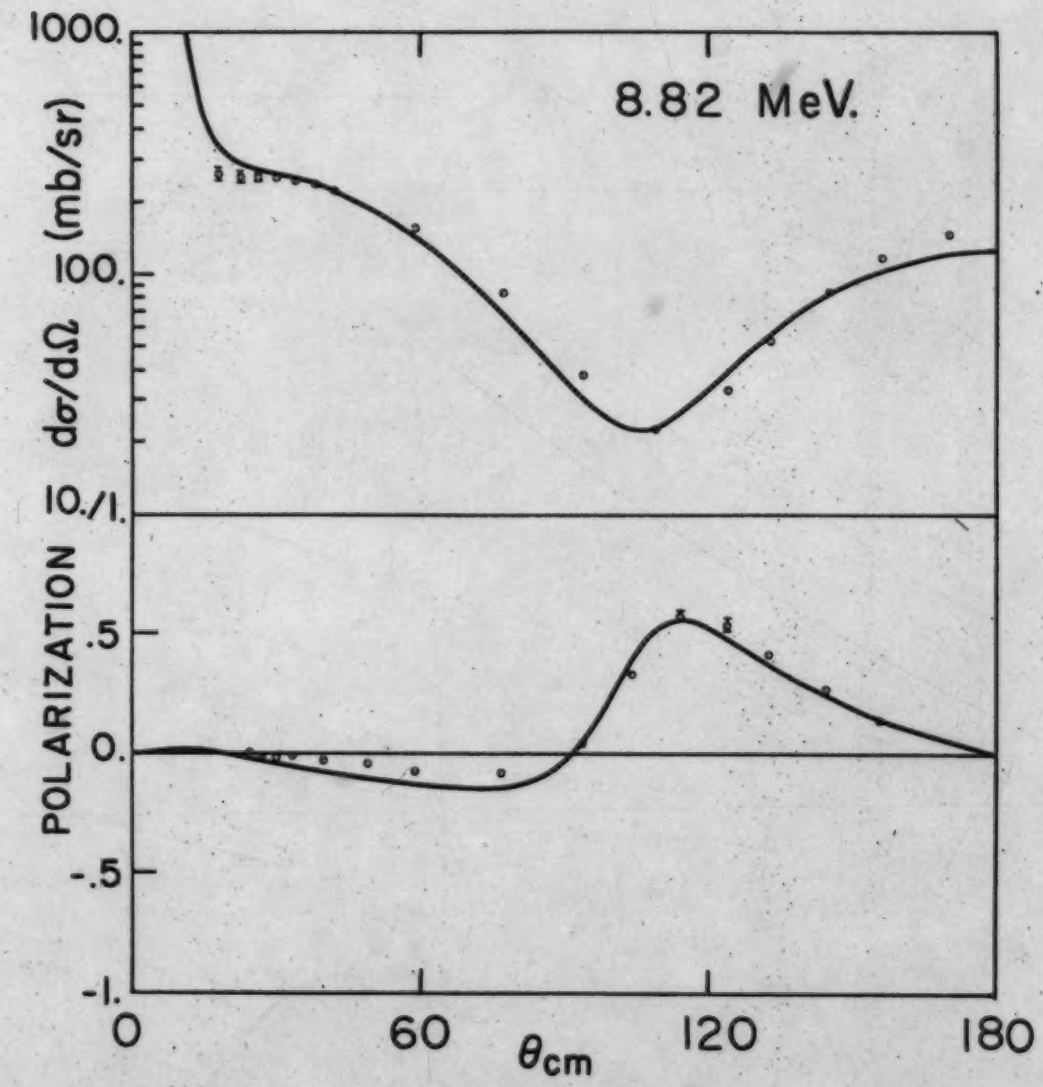

Figure 13 Optical model fit to 8.82 MeV p + ^{3}He scattering data (Mc64,Mo69).

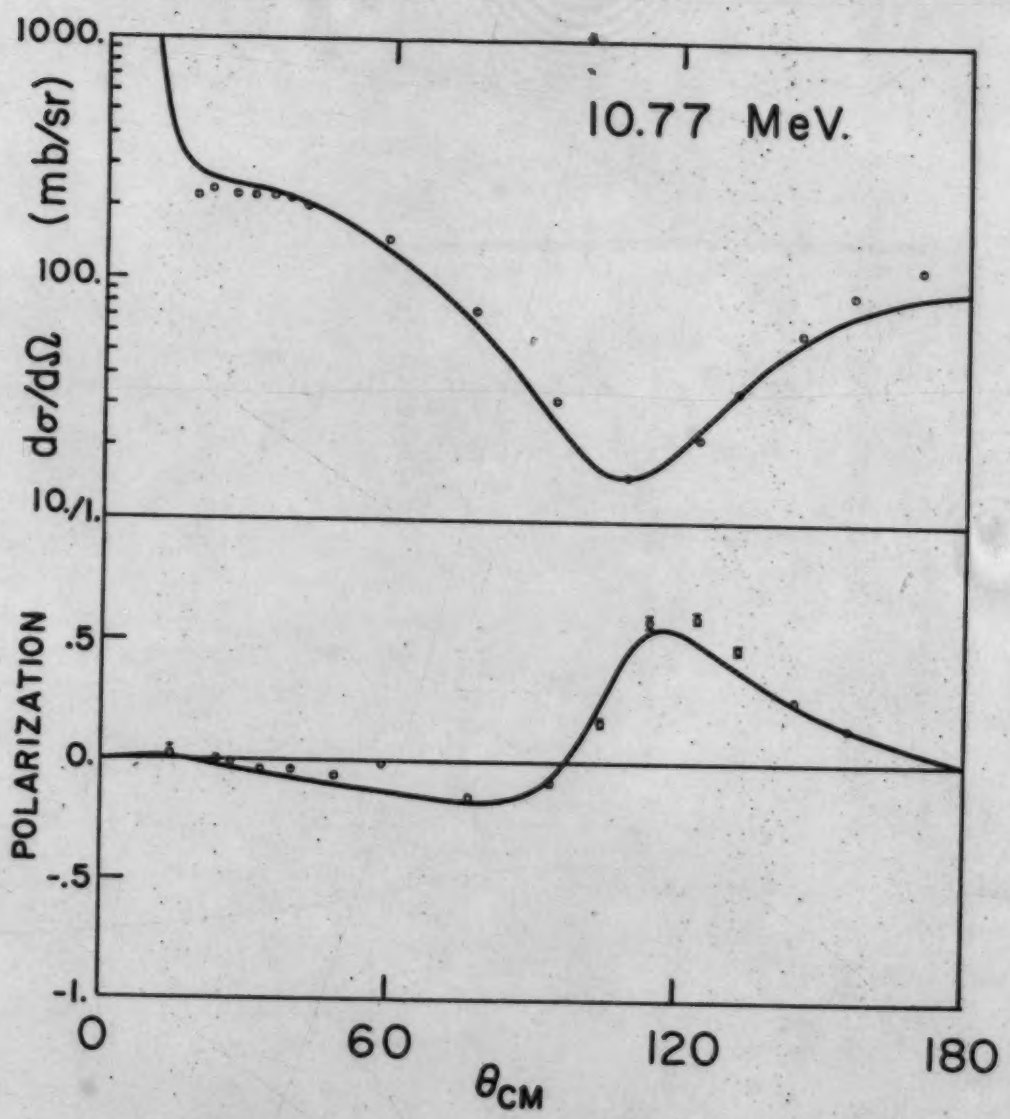

Figure 14 Optical model fit to 10.77 MeV p + ^{3}He scattering data (Mc64, Mo69).

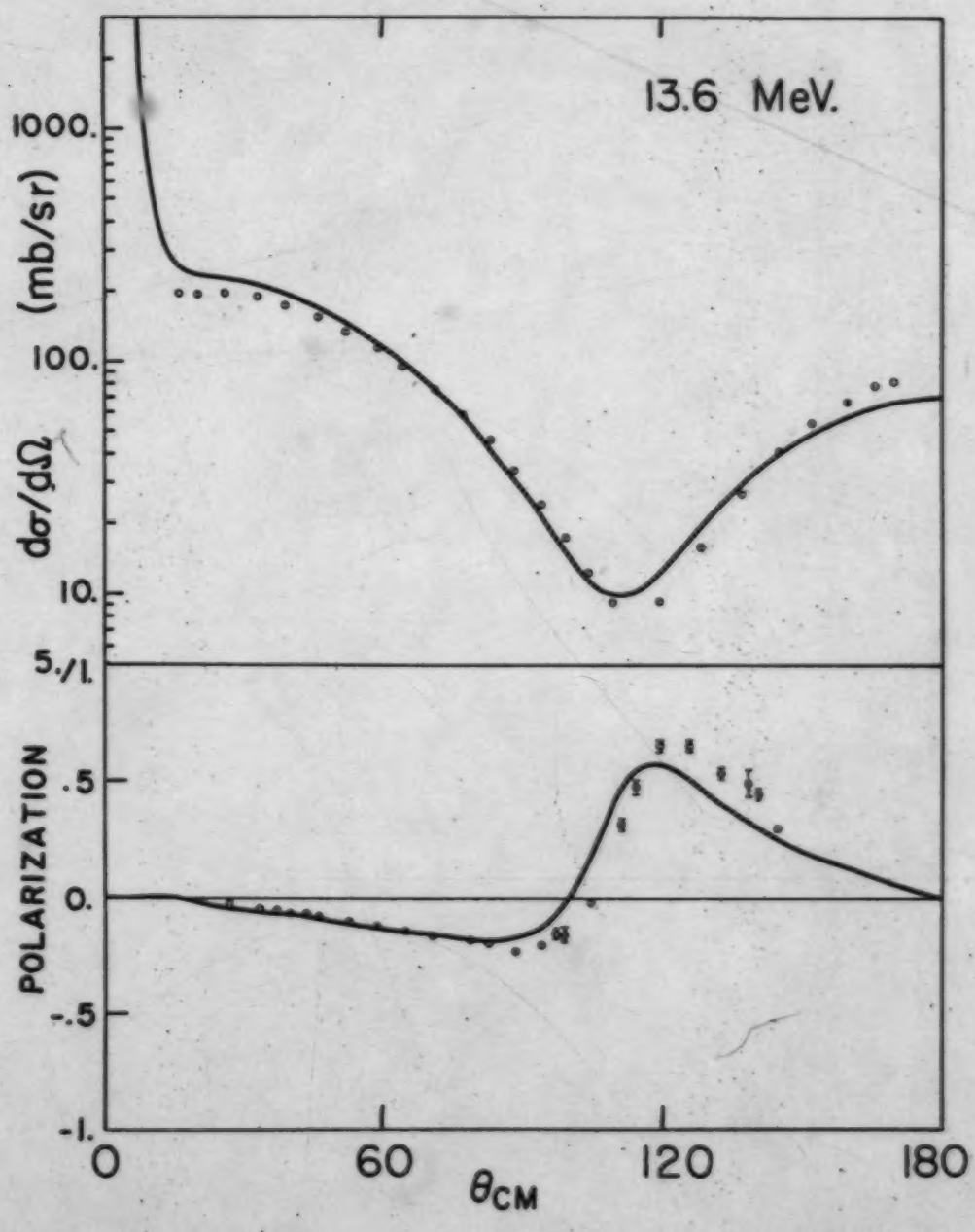

Figure 15 Optical model fit to 13.6 MeV p + ^{3}He scattering data (Hu71, Ti68).

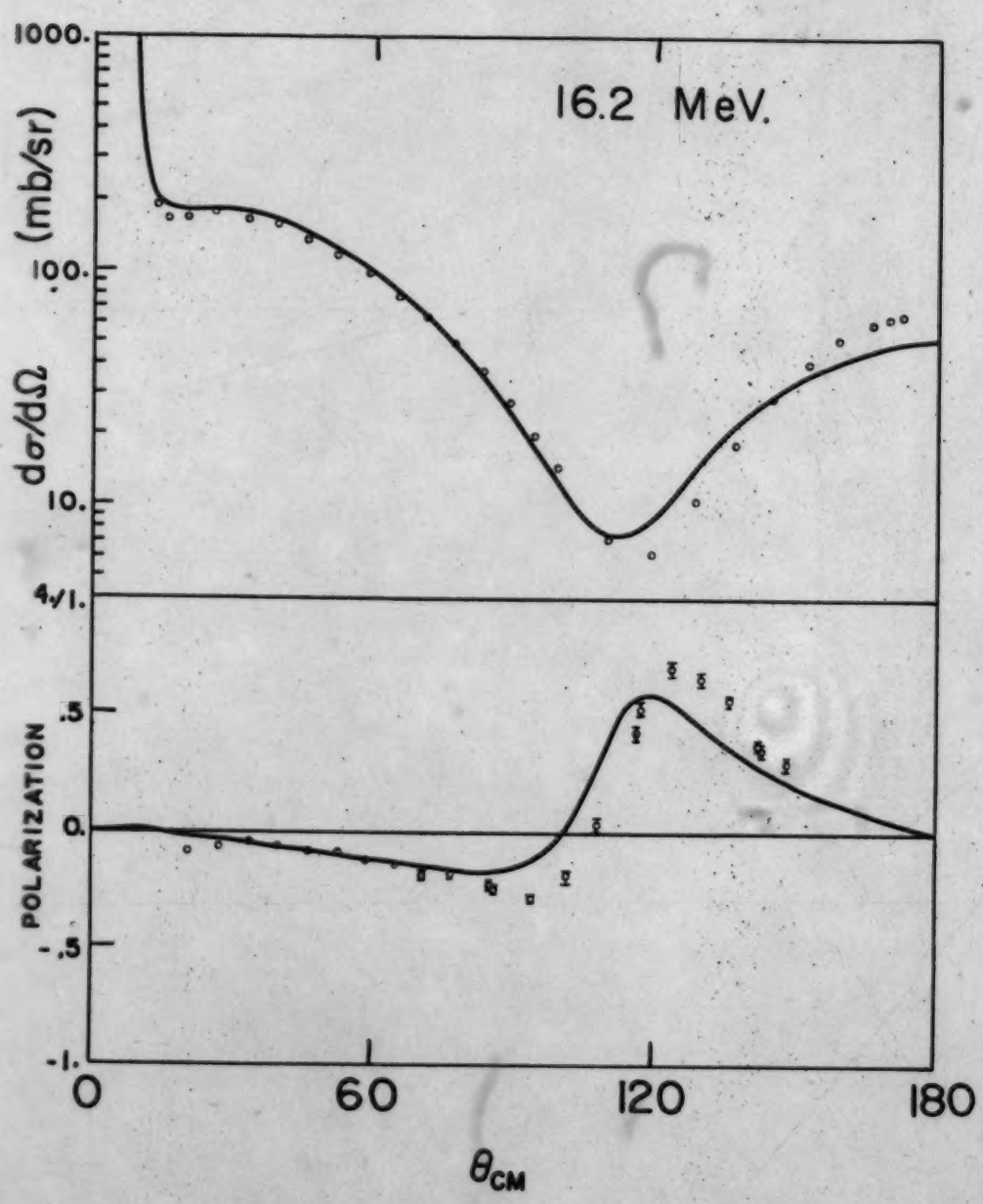

Figure 16 Optical model fit to 16.2 MeV p + ^{3}He scattering data (Hu71, Ti68).

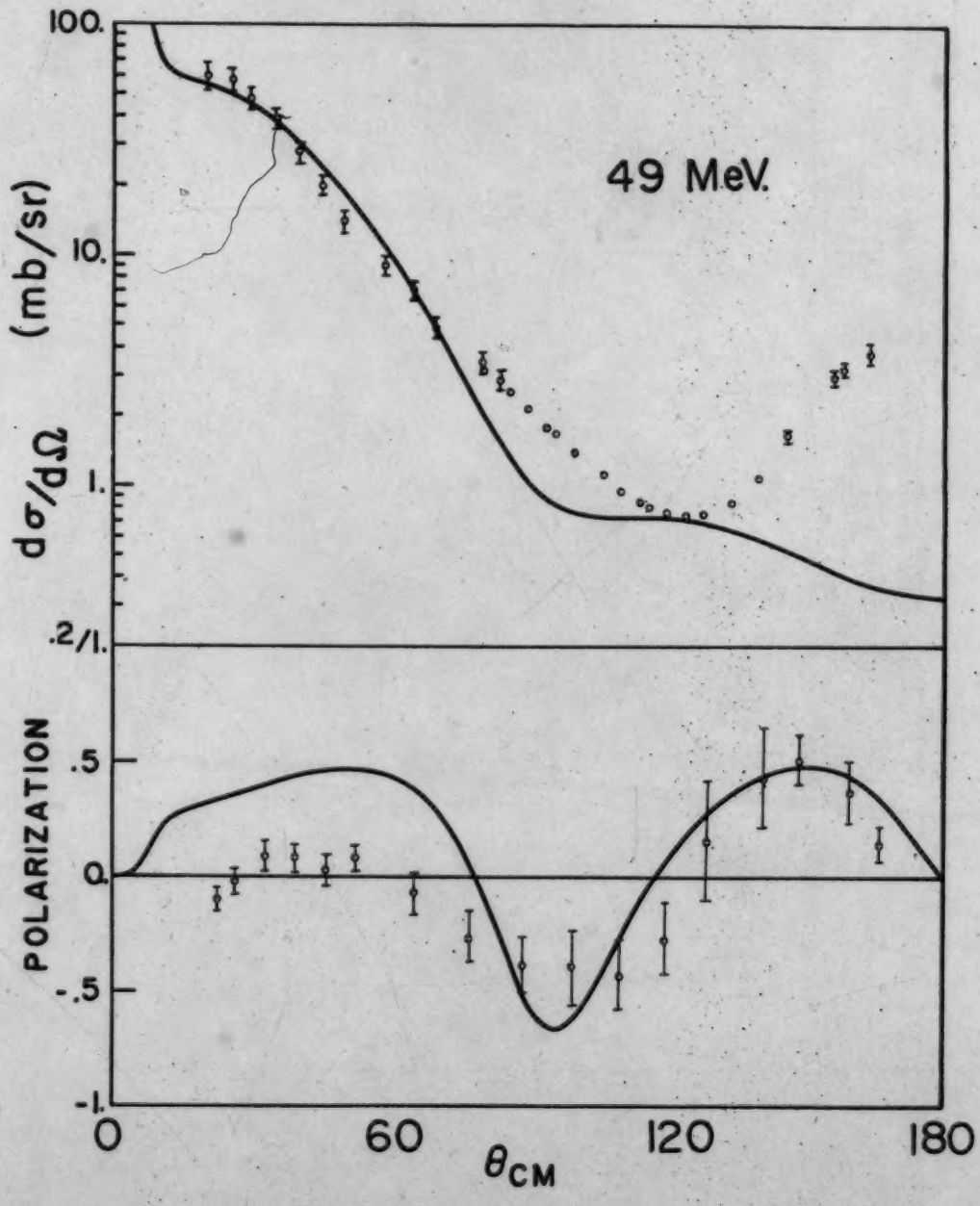

Figure 17 Optical model fit to 49 MeV p + ^{3}He scattering data (Ha70, Mo70).

CHAPTER 6

EXCHANGE

The standard optical model cannot easily explain the large backward scattering cross sections observed. This is clear from the figures presented in Chapter 5. From the resonating group studies we find that when the wave function is antisymmetrized; the large back angle scattering can be reproduced. Thompson and Tang (Th71) found that the resonating group formalism leads to a differential equation containing a direct scattering potential as well as three additional terms. These three terms correspond to (a) nucleon exchange (knock out) (b) heavy particle pick up and (c) "nucleon-rearrangement" (see Figure 18). Using the first Born approximation they found that (a) is forward peaked and (b) and (c) are backward peaked. These can be replaced in the Born approximation by equivalent energy dependent potentials. Thus, (b) and (c) give rise to a Majorana exchange with a $(-1)^{\ell}$ dependence.

Greenlees and Tang (Gr71) performed the following calculation to obtain a form suitable to use in an optical model analysis. Recall from resonating group studies:

$$\left(\frac{-\hbar^2}{2\mu}\nabla^2 + E - V_D(r) - V_c(r)\right)\psi(r) = \int K(\underset{\sim}{r},\underset{\sim}{r}')\psi(\underset{\sim}{r})d\underset{\sim}{r}' \qquad (6.1)$$

where μ is the reduced mass of the particles, E is the relative energy of the nuclei in the center of mass frame; V_c is the coulomb potential; V_D is the direct potential, and $K(\underset{\sim}{r},\underset{\sim}{r}')$ is the kernel function which contains additive terms of the type:

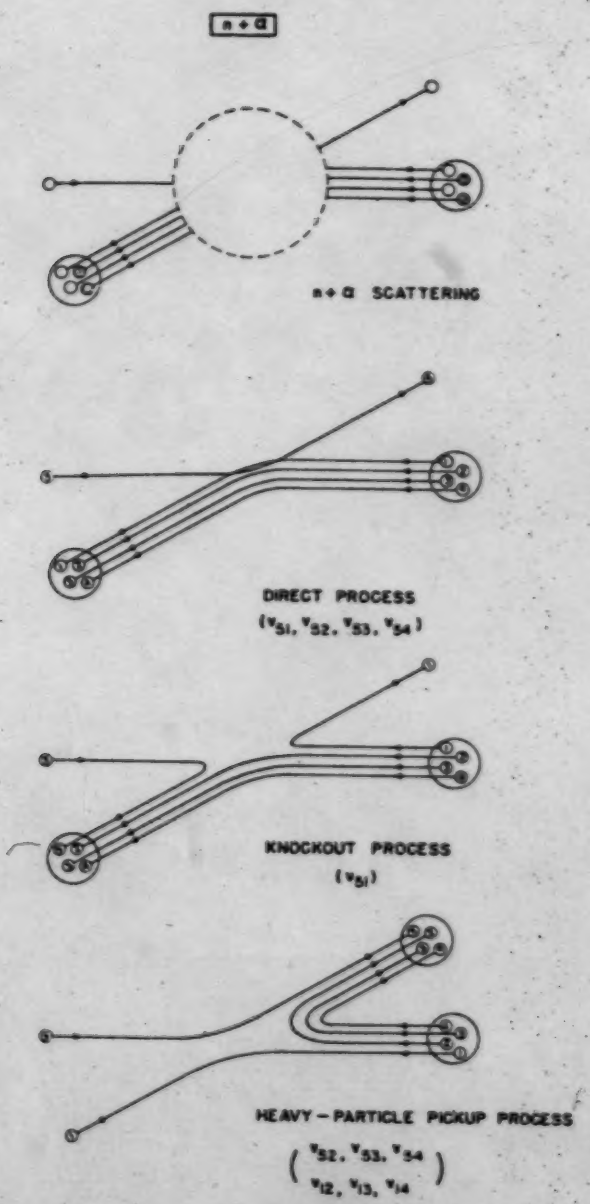

Figure 18 Schematic representation of the n + α scattering problem as a sum of direct and exchange processes. The nucleon-rearrangement process is not shown.

$$K_1(\underset{\sim}{r},\underset{\sim}{r}') = g_1(r,r')\exp[-\beta_1(\underset{\sim}{r}-\underset{\sim}{r}')^2] \tag{6.2}$$

$$K_2(\underset{\sim}{r},\underset{\sim}{r}') = g_2(r,r')\exp[-\beta_2(\underset{\sim}{r}+\underset{\sim}{r}')^2] \tag{6.3}$$

where g_1 and g_2 are form factors symmetric in $\underset{\sim}{r}$ and $\underset{\sim}{r}'$, and β_1 and β_2 are non-local range parameters.

Since the antisymmetrization procedures may be important for heavier systems it is reasonable to assume that the general non-local optical potential should contain a direct potential V_D as well as a kernel of the form:

$$K(\underset{\sim}{r},\underset{\sim}{r}') = K_1(\underset{\sim}{r},\underset{\sim}{r}') + K_2(\underset{\sim}{r},\underset{\sim}{r}') \tag{6.4}$$

$$= g_1(r,r')e^{-\beta_1(\underset{\sim}{r}-\underset{\sim}{r}')^2} + g_2(r,r')e^{-\beta_2(\underset{\sim}{r}+\underset{\sim}{r}')^2} \tag{6.5}$$

where the second term has not been previously considered in non-local optical models, it is particularly important in scattering at backward angles.

Let f_D, f_1 and f_2 be the scattering amplitudes corresponding to the potentials V_D, K_1, and K_2. At high enough energies, one may use the Born approximation to calculate these:

$$f_D = -\frac{\mu}{2\pi\hbar^2}\int\exp(-i\underset{\sim}{k}_f\cdot\underset{\sim}{r})V_D(r)\exp(i\underset{\sim}{k}_i\cdot\underset{\sim}{r})d\underset{\sim}{r} \tag{6.6}$$

$$f_1 = -\frac{\mu}{2\pi\hbar^2}\int\exp(-i\underset{\sim}{k}_f\cdot\underset{\sim}{r})K_1(\underset{\sim}{r},\underset{\sim}{r}')\exp(i\underset{\sim}{k}_i\cdot\underset{\sim}{r})d\underset{\sim}{r}\, d\underset{\sim}{r}' \tag{6.7}$$

$$f_2 = -\frac{\mu}{2\pi\hbar^2}\int\exp(i\underset{\sim}{k}_f\cdot\underset{\sim}{r})K_2(\underset{\sim}{r},\underset{\sim}{r}')\exp(i\underset{\sim}{k}_i\cdot\underset{\sim}{r})d\underset{\sim}{r}\, d\underset{\sim}{r}' \tag{6.8}$$

where $\underset{\sim}{k}_i$, and $\underset{\sim}{k}_f$ are the initial and final wave vectors.

Now f_D is large only in the forward direction if V_D is smoothly varying, and f_1 and f_2 can be written:

$$f_{1,2} = -\frac{\mu}{2\pi\hbar^2}\int \exp[\tfrac{i}{2}(\underset{\sim}{k}_f+\underset{\sim}{k}_i)\cdot(\underset{\sim}{r}'-\underset{\sim}{r})]$$

$$\exp[\tfrac{i}{2}(\underset{\sim}{k}_i-\underset{\sim}{k}_f)(\underset{\sim}{r}'+\underset{\sim}{r})]K_{1,2}(\underset{\sim}{r},\underset{\sim}{r}')d\underset{\sim}{r}\, d\underset{\sim}{r}' \quad . \tag{6.9}$$

At forward angles where $\underset{\sim}{k}_i \approx \underset{\sim}{k}_f$ the contributions to f_1 and f_2 come mainly from the integration region where $\underset{\sim}{r} \approx \underset{\sim}{r}'$; therefore f_1 is important at forward angles and f_2 is not, since $K_1 >> K_2$. At backward angles where $\underset{\sim}{k}_i \approx -\underset{\sim}{k}_f$ the contributions to the scattering amplitudes are mainly from the integration region $\underset{\sim}{r} \approx -\underset{\sim}{r}'$ where $K_1 << K_2$. Hence, f_2 is important at backward angles and f_1 is not.

As an example, choose:

$$V_D = -V_{D0}\exp[-\alpha_D r^2] \tag{6.10}$$

$$g_1 = -g_{10}\exp[-\alpha_1(r^2+r'^2)] \tag{6.11}$$

$$g_2 = -g_{20}\exp[-\alpha_2(r^2+r'^2)] \tag{6.12}$$

these yield:

$$f_D = \frac{\mu}{2\pi\hbar^2} V_{D0}\left(\frac{\pi}{\alpha_D}\right)^{3/2}\exp\left(\frac{-(\underset{\sim}{k}_f-\underset{\sim}{k}_i)^2}{4\alpha_D}\right) \tag{6.13}$$

$$f_1 = \frac{\mu}{2\pi\hbar^2} g_{10}\left(\frac{\pi^2}{\alpha_1(\alpha_1+2\beta_1)}\right)^{3/2}\exp\left(\frac{-(\underset{\sim}{k}_f+\underset{\sim}{k}_i)^2}{8\alpha_1+16\beta_1}\right)\exp\left(\frac{(\underset{\sim}{k}_f-\underset{\sim}{k}_i)^2}{8\alpha_1}\right) \tag{6.14}$$

$$f_2 = \frac{\mu}{2\pi\hbar^2} g_{20}\left(\frac{\pi^2}{\alpha_2(\alpha_2+2\beta_2)}\right)^{3/2} \exp\left[\frac{-(k_f+k_i)^2}{8\alpha_2}\right] \exp\left[\frac{-(k_f-k_i)^2}{8\alpha_2+16\beta_2}\right] \tag{6.15}$$

verifying the above conclusion. (Note that the resonating group studies indicate that $g_1 \simeq g_2$ and $\beta_1 \simeq \beta_2$).

Therefore, it is important to include a K_2 type kernel in the non-local optical potential to account for large backward angle cross sections.

For local potentials, we note, in the Born approximation, that f_1 and f_2 in Equations (6.14) and (6.15) are also the scattering amplitudes of the potentials:

$$V_1(r) = -g_{10}\left(\frac{\pi}{\beta_1}\right)^{3/2} \exp\left[-\frac{1}{2}\frac{k^2}{\alpha_1+2\beta_1}\right] \exp\left[-\frac{\alpha_1}{\beta_1}(\alpha_1+2\beta_1)r^2\right] \tag{6.16}$$

$$V_2(r) = -g_{20}\left(\frac{\pi}{\beta_2}\right)^{3/2} \exp\left[-\frac{1}{2}\frac{k^2}{\alpha_2+2\beta_2}\right] \exp\left[-\frac{\alpha_2}{\beta_2}(\alpha_2+2\beta_2)r^2\right] P^r \tag{6.17}$$

where $k = |\underset{\sim}{k}_i| = |\underset{\sim}{k}_f|$ and P^r is the Majorana operator (space exchange). This suggests that, it may be possible to simulate the exchange effect by allowing the optical potential to contain a Majorana component. Thus we may write:

$$V = V_a(r) + V_b(r)\, P^r \quad . \tag{6.18}$$

A simpler, but cruder alternative is:

$$V = (a + b P^r) V_D(r) \tag{6.19}$$

where V_a and V_b are smoothly varying potentials, with a and b as adjustable energy dependent parameters.

Clearly, the addition of a term of $(-1)^{\ell}$ dependence can produce a rise in the back angle cross section since it can reduce the cancellation of the alternate Legendre polynomials in the backward angles.

In the present work, the exchange terms were included in the potentials in the following way:

$$\begin{aligned} V_o &\rightarrow V_o[1 + C_o(-1)^{\ell}] \\ W_v &\rightarrow W_v[1 + C_v(-1)^{\ell}] \\ V_{so} &\rightarrow V_{so}[1 + C_{so}(-1)^{\ell}] \quad . \end{aligned} \tag{6.20}$$

The exchange term is included in the imaginary component since it has been found necessary, by other authors (Br72, Th73) to obtain a good fit. These terms were incorporated into the computer code TASHTASH.

The $n + {}^3H$ case was not analysed with the exchange terms since the data does not extend into the backward angles, sufficiently. A manual search was performed over all the $p + {}^3He$ data sets. Significant improvements were observed for only two energies, 30 MeV and 156 MeV, which are shown in Figures 19 and 20. Improvements for the other energies were not as impressive. The case of the 19.4 MeV curve is shown in Figure 21. The values obtained for the exchange parameters are given in Table 5. Figures 22 through 27 show the individual effects of C_o, C_v and C_{so}, for 30 MeV and 156 MeV in comparison with the pure optical model fits. (Note that the optical model parameters did not change when searched upon once the exchange parameters had been determined.)

TABLE 5

EXCHANGE PARAMETERS FOR P + ^{3}HE

E_n (MeV)	C_o (MeV)	C_v (MeV)	C_{so} (MeV)	x_σ^2 / N_σ	x_p^2 / N_p
19.4	0.0	0.0	0.0	303.1	248.8
19.4	-0.012	-0.25	0.0	340.8	61.3
30.0	-0.065	-0.4	0.06	25.2	1.6
156	-0.066	0.007	0.023	74.5	24.9

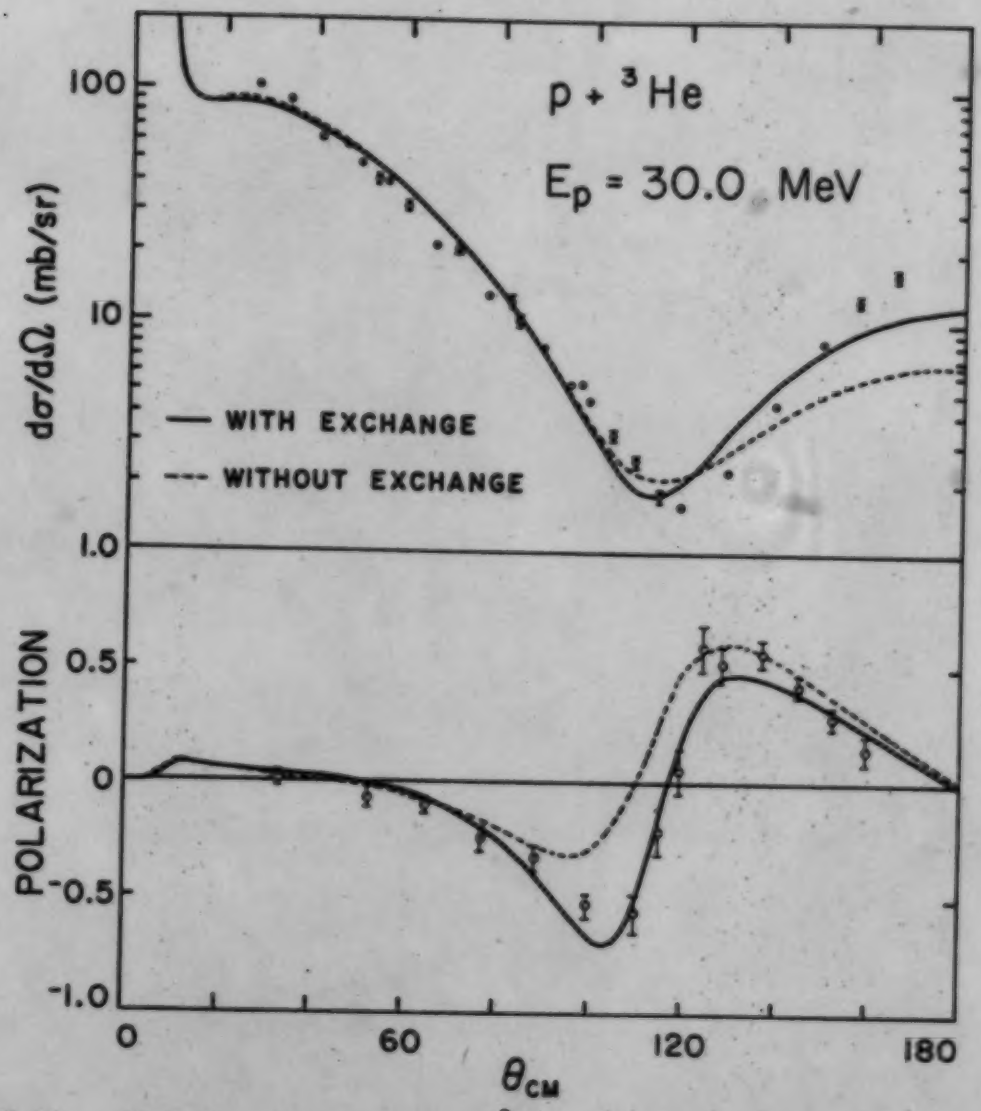

FIGURE 19: Optical model fits for p + ^{3}He at 30 MeV with and without exchange. Data (Ha70, Mo70, Ha68).

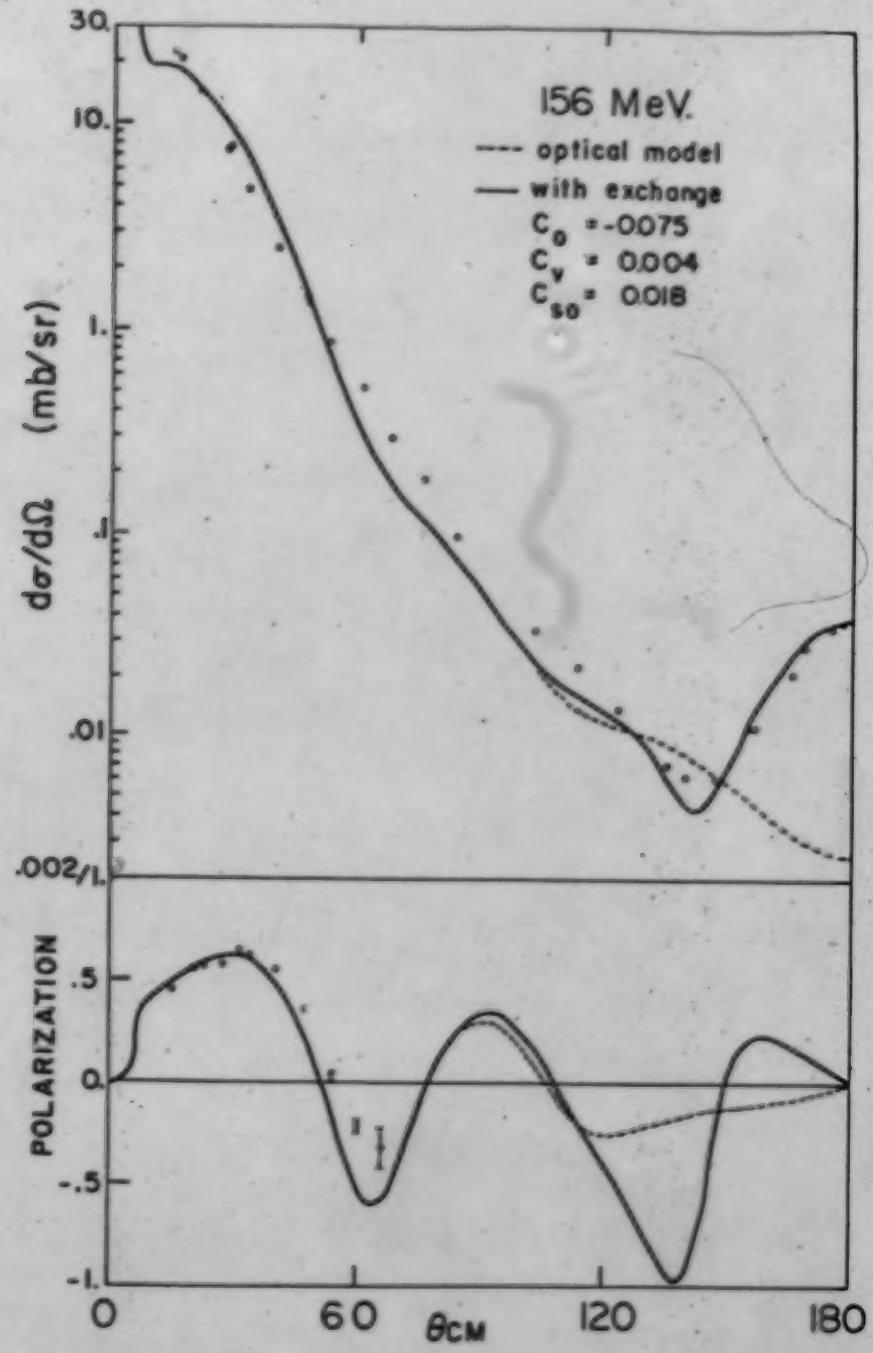

Figure 20 Optical model fits for p + ^{3}He at 156 MeV with and without exchange. Data (La70, Frpc).

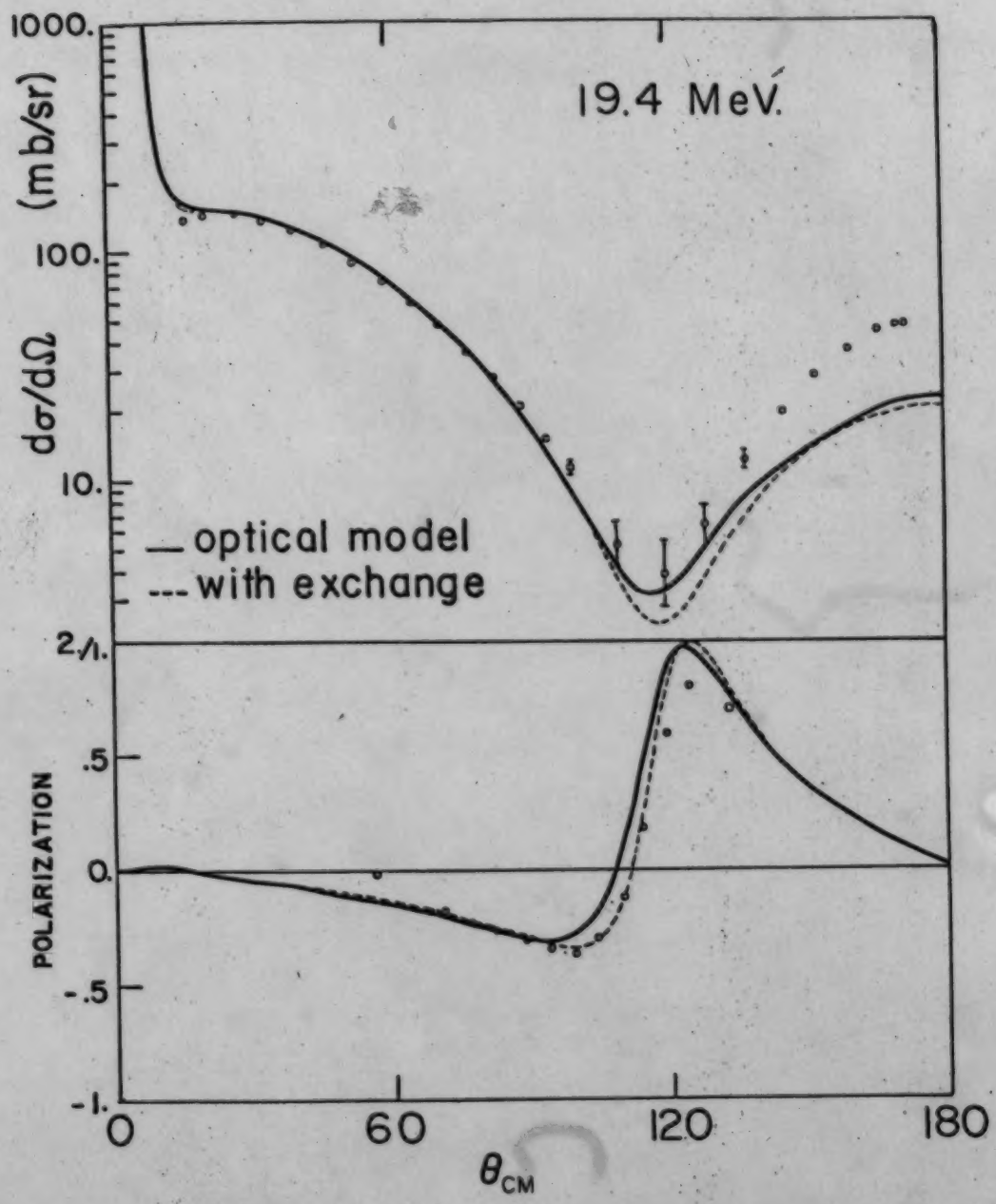

Figure 21 Optical model fits for p + ^{3}He at 19.4 MeV with and without exchange. Data (Ba71).

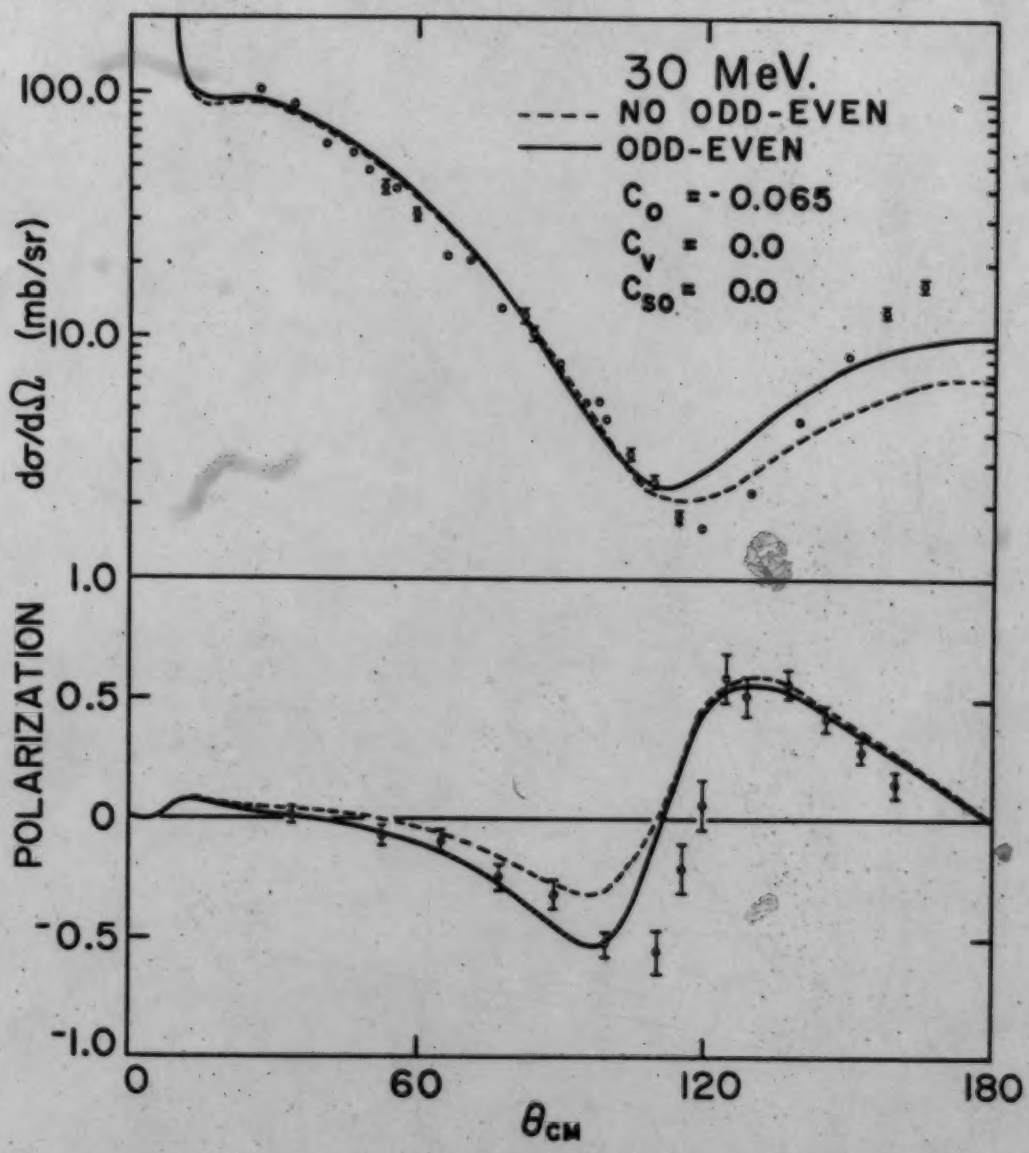

FIGURE 22: Optical model fits for p + ^{3}He at 30 MeV with C_o = -0.065 MeV and without exchange.

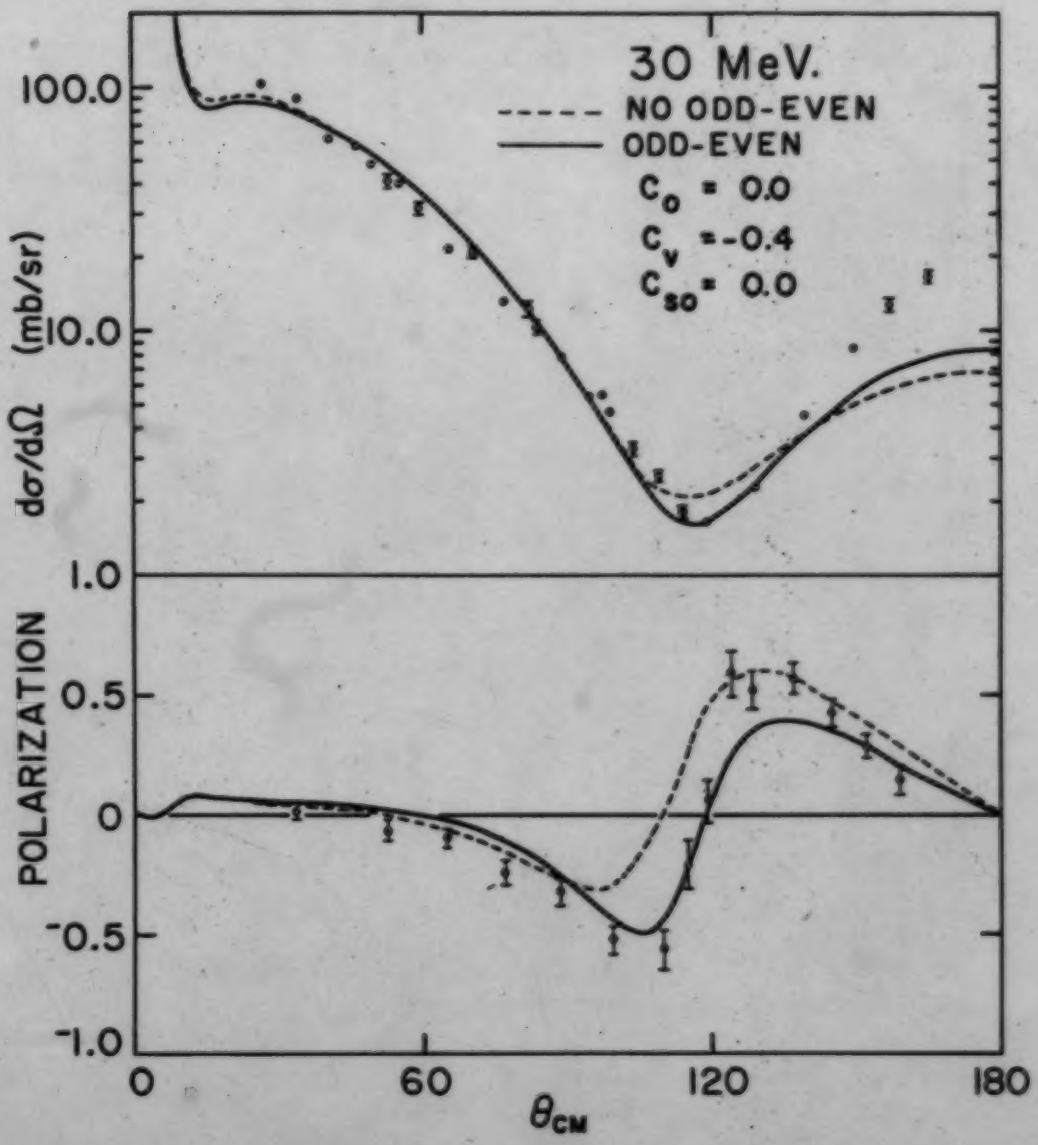

FIGURE 23: Optical model fits for p + ^{3}He at 30 MeV with C_v = -0.4 MeV and without exchange.

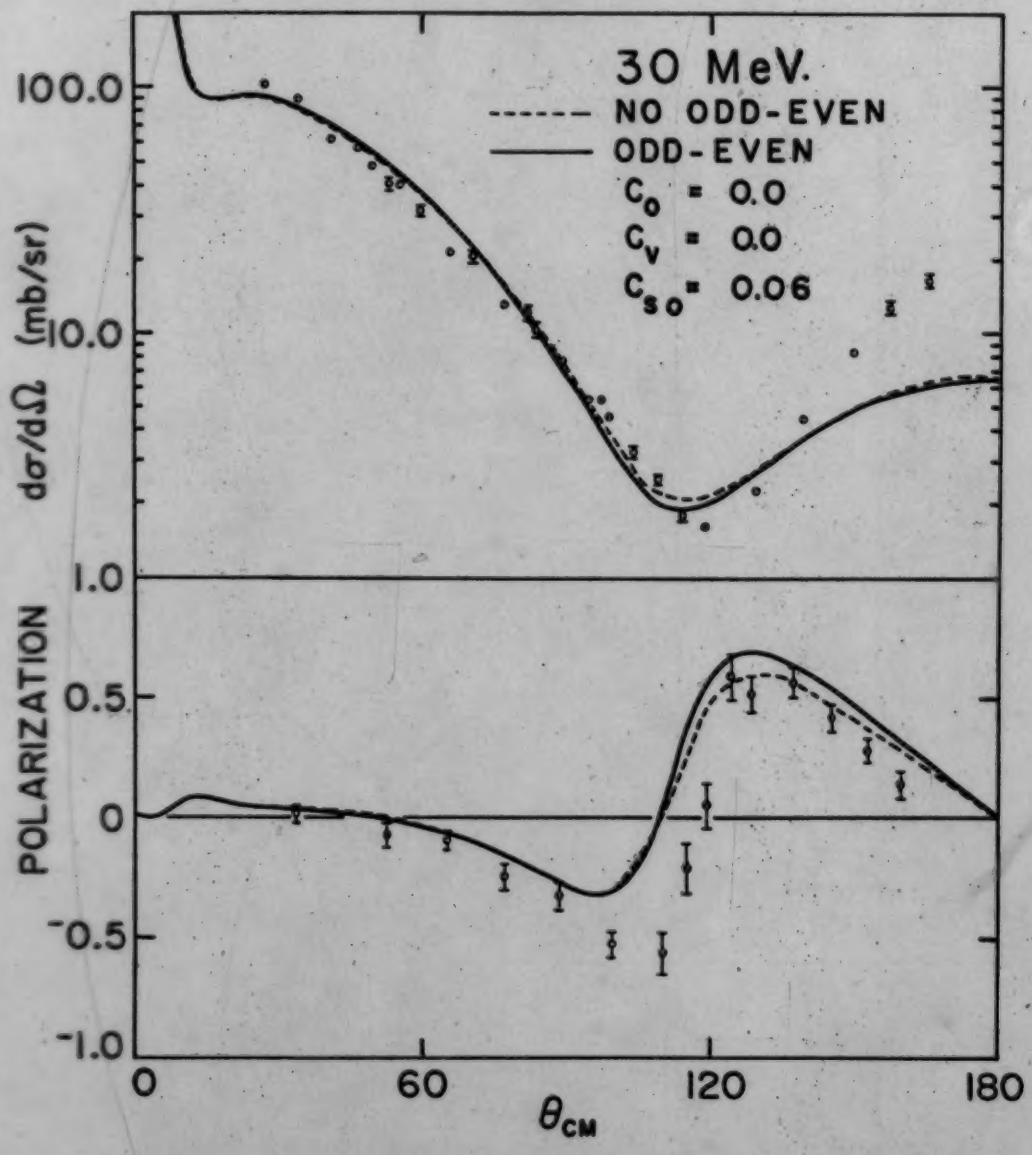

FIGURE 24: Optical model fits for p + ^{3}He at 30 MeV with C_{so} = 0.06 MeV and without exchange.

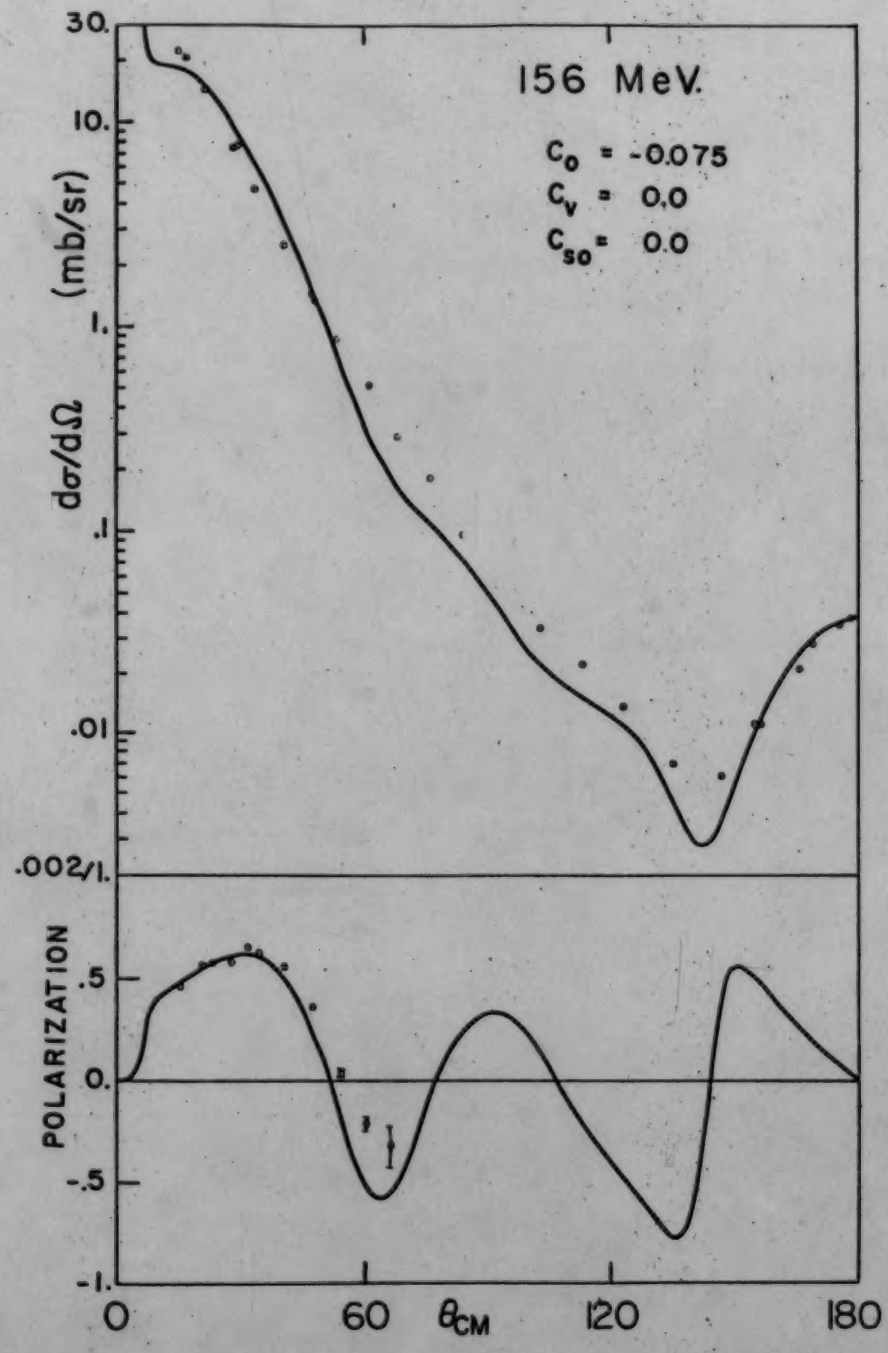

FIGURE 25: Optical model fit for p + ^{3}He at 156 MeV with C_0 = -0.075 MeV.

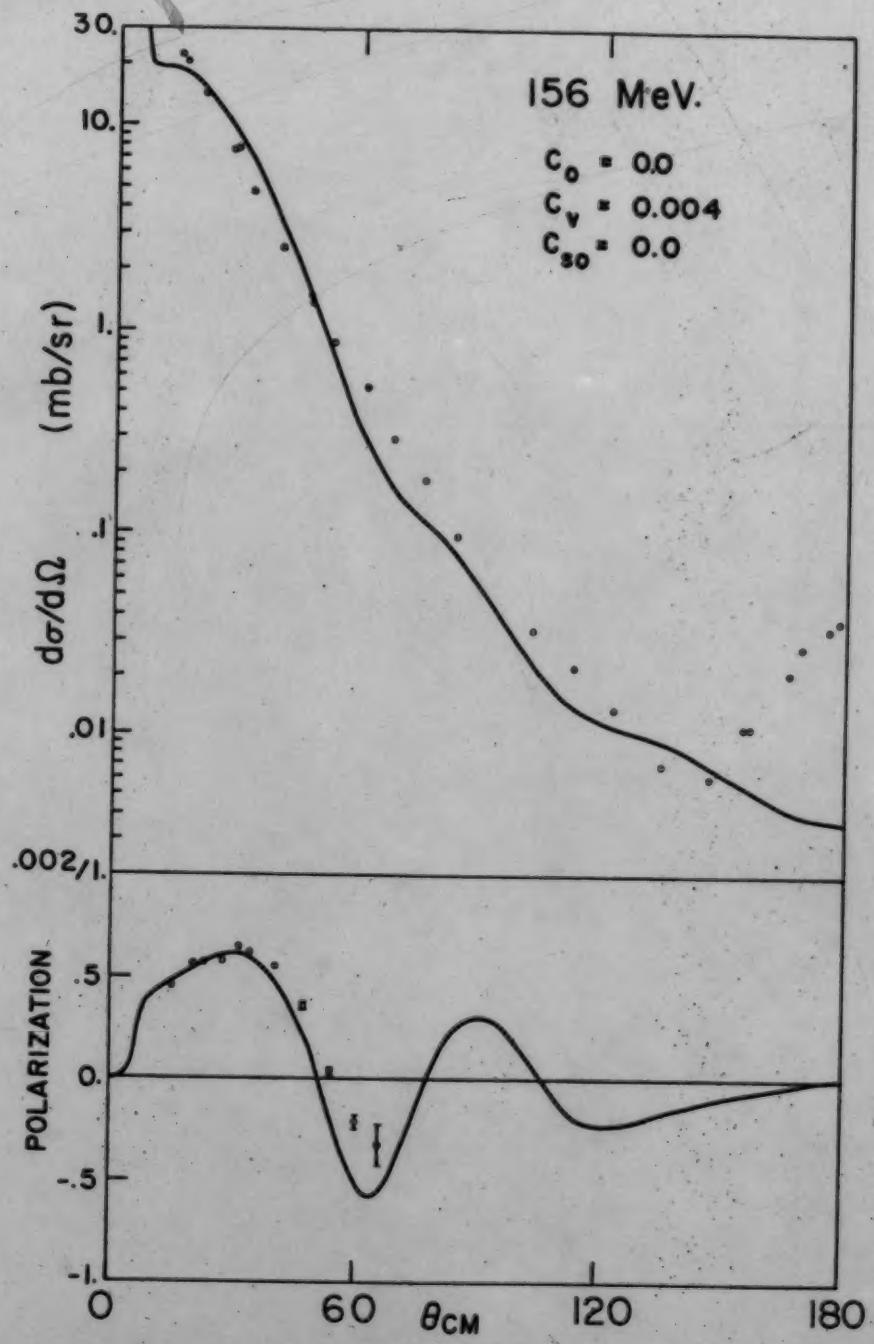

FIGURE 26: Optical model fit for p + ^{3}He at 156 MeV with C_v = 0.004 MeV.

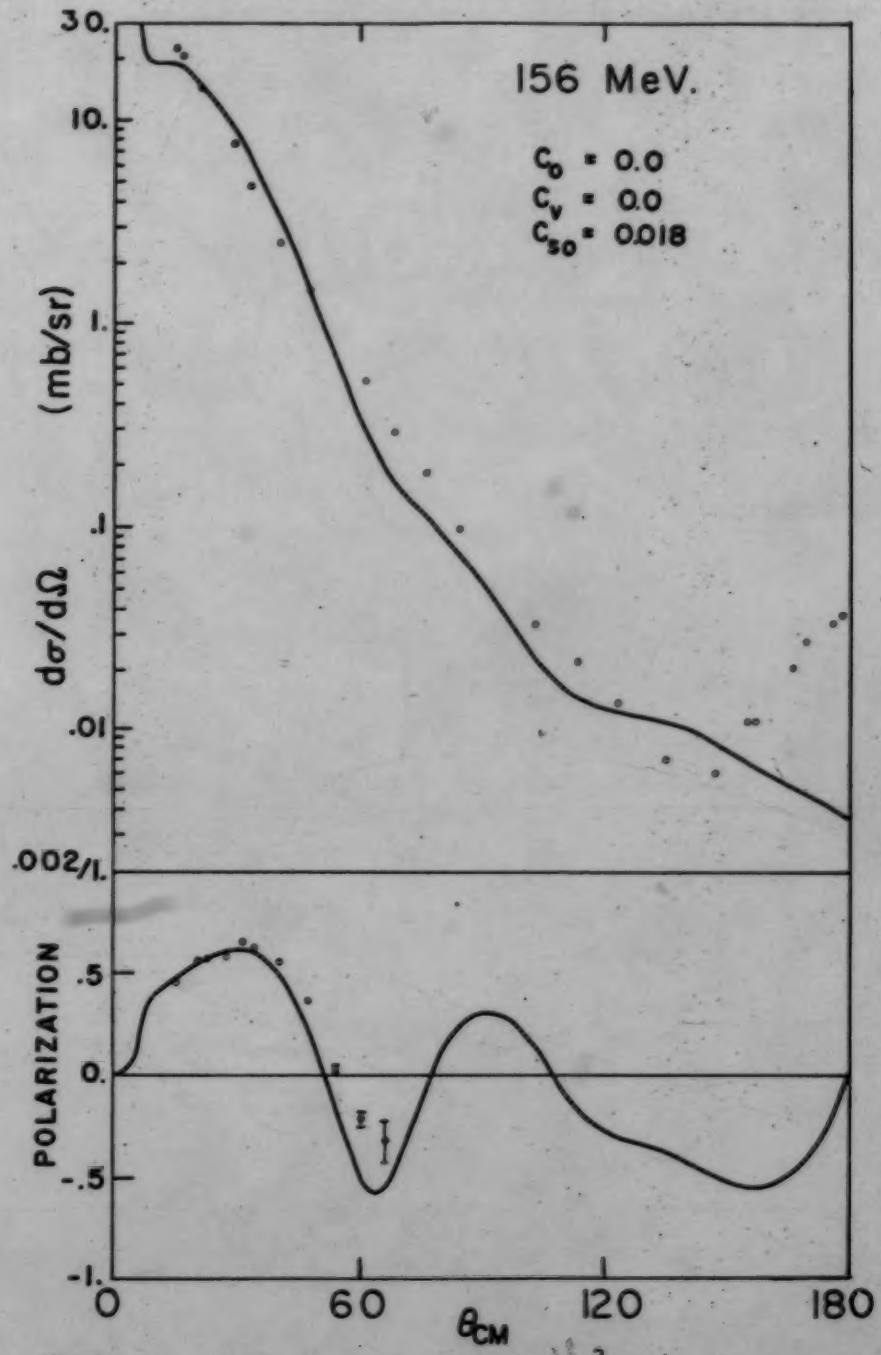

FIGURE 27: Optical model fit for p + ^{3}He at 156 MeV with C_{so} = 0.018 MeV.

In the 30 MeV and 156 MeV cases, a marked rise in the differential cross section at backward angles is observed when the exchange is included. For the 30 MeV polarization, the exchange improved the fit tremendously. For the 19.4 MeV, the exchange improved the fit to the polarization, however, the fit to the differential cross section was made worse. For energies where this disagreement occured, the exchange yielded no overall improvement and was, therefore, left out in the best fit. From Figures 22 through 27, one sees that the C_o and C_v were the major contributors in the backward angle cross section increases. Also these were the major contributors in improving the 30 MeV polarization fit.

CHAPTER 7

DISCUSSION AND CONCLUSION

DISCUSSION

In this section, comparisons will be made between the curves obtained by the various analysis methods and the optical model. Exchange in the optical model will also be considered.

$n + {}^3H$

All the discussed analysis methods were performed for this system on the differential cross section at 6 MeV. The optical model curve is one of the better fits to the data. All the available differential cross section data for this system have been analysed by LeMere et al (Le75) and ourselves (Sh72). Over the whole data set the optical model fits are at least as good as the resonating group fits. We also analysed the only polarization data available, at 22.1 MeV, and achieved a good fit.

One must note that no data sets were available for which there was polarization as well as differential cross section data. This does allow better fits since in many cases the polarization data requires the parameters to go in a different direction than the cross section data requires. This is not too serious a problem in this case since the parameters obtained at 21 MeV are not very much different from those obtained at 21 MeV and 23 MeV (see Table 4).

On the whole, the optical model gave very satisfactory fits to the available experimental data from 6 MeV to 23 MeV, for $n + {}^3H$ elastic scattering.

For the p +^{3}He system, there exists a great deal of data, therefore, the analysis was restricted to energies for which both polarization and differential cross section data were available, i.e. from 5.51 MeV to 156 MeV. Note that the well geometry used is the same as for the n +^{3}H system.

The agreement between the model predictions and the data is good, with the exception of 49 MeV, for which a good fit could not be obtained with reasonable parameters. Inspection of Table 4 (for both p +^{3}He and n +^{3}H) reveals the following trends in the potential depths:

(1) The real well depth decreased uniformly as the energy increases.

(2) The imaginary volume well depth, W_V, increased in general, as expected.

(3) The imaginary surface well depth, W_D, was kept at zero for the best fit.

(4) The spin-orbit well depth increased smoothly with energy.

A quadratic least squares fit was performed on the variation of the real well depth with energy. The resulting equation is:

$$V_o(E) = 53.75 - 0.869\ E + 0.004\ E^2 \qquad (7.1)$$

This equation can be compared with those obtained by other authors, for proton scattering from:

^{4}He (Sa68): $V_o(E) = 53.3 - 0.69\ E$ (7.2)

Medium-heavy nuclei (Ro66): $V_o(E) = 53.8 - 0.33\ E$ (7.3)

It appears that as the mass of the target nucleus decreases, the slope of the curve becomes steeper. Also, note that if a linear fit was used

for the p +^{3}He case, the slope would have been somewhat flatter (and the fit not nearly as good). See Figure 28 for the plot of Equation (7.1).

The exchange effect made a marked improvement in the 30 MeV and 156 MeV optical model fits. The fits obtained including non-zero exchange terms for the other energies did not really improve the curves.

The 49 MeV case has presented many problems since it refuses to be fit decenty. This leads one to believe that the data maybe incorrect, however the 48.5 MeV differential cross section data agrees almost exactly with the 49.5 MeV data. Note that in the 49 MeV analysis, 49.0 MeV polarization data was analysed with 49.5 MeV differential cross section data. It is not at all clear what is the problem at this energy.

Comparing the microscopic calculation fits for polarization and differential cross section for 5.51 MeV to 10.77 MeV with the optical model fits, one finds that the microscopic calculation fits are better at lower energies and equivalent for the higher energies. The optical model does have an advantage since it is easily extended to higher energies where the microscopic calculations are not. The optical model fits are superior to the resonating group fits for energies less than 12 MeV, with the advantage that it can handle the polarization data that the resonating group cannot. Comparing the phase shift analysis of p +^{3}He at 30 MeV with the optical model analysis, one finds that the phase shift analysis obtained five equivalent type 1 fits, all of which were better than the optical model curves (with and without exchange). However, the phase shift method required nineteen parameters and obtained at least four extraneous solutions which cannot be eliminated. Whereas, the optical model fits are good and the problem of extraneous solutions

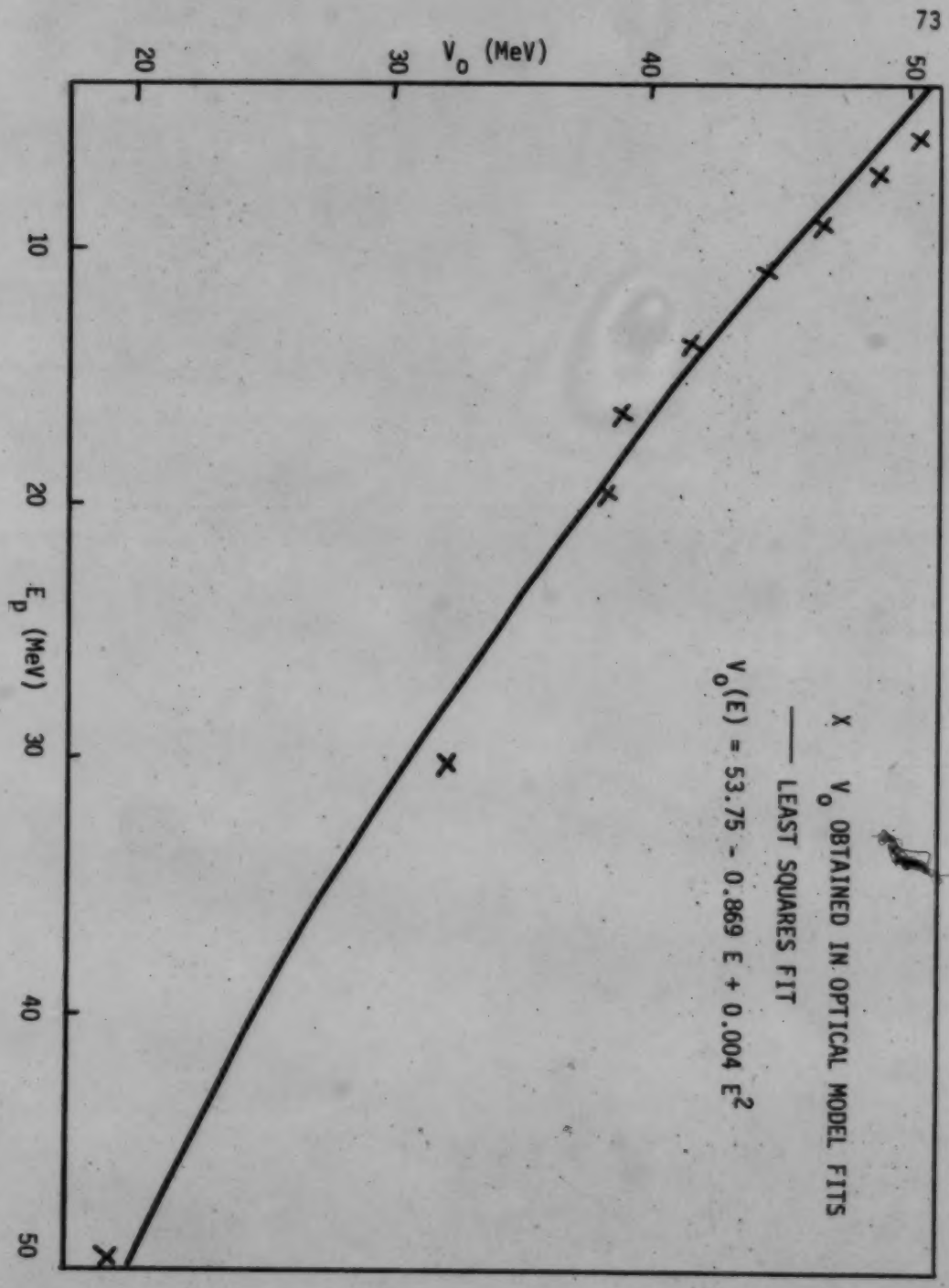

Figure 28 Least squares fit to the V_o's obtained from the optical model fit for p + ^{3}He; yielding the equation:

$$V_o(E) = 53.75 - 0.869\ E + 0.004\ E^2$$

does not exist.

CONCLUSION

This work was undertaken in order to demonstrate the usefulness of the optical model as an analysis method for scattering off very light nuclei. We have found that it yields fits which are comparable or superior to the standard methods. The optical model is more useful than the resonating group method (also microscopic calculations) in analysis over a broad energy range. It is easier to use than phase shift analysis since it does not employ as many parameters or obtain extraneous solutions.

We believe that the optical model is a valid semi-phenomenological analysis method for the elastic scattering of nucleons off very light nuclei, and when coupled with exchange terms becomes a very useful tool indeed.

A logical extention to this work would be to include spin-spin terms in the potential in order to determine their importance.

REFERENCES

Ba 71 S.D. Baker et al, Nucl Phys A160 (1971) 428

Bi 52 L.C. Biedenharn, J.M. Blatt, M.E. Rose, Rev Mod Phys 24 (1952) 249

Br 72 Ronald E. Brown, Y.C. Tang, D.R. Thompson, in "Few Particle Problems in the Nuclear Interaction" edited by I. Slaus (North-Holland, Amsterdam,1972) 703

Cl 64 T.B. Clegg et al, Nucl Phys 50 (1964) 621

De 72 R.M. Devries et al, Nucl Phys A188 (1972) 449

Ei 66 H. Eikemeier, H.H. Hackenbroich, Z. Physik 195 (1966) 412

Fr pc R. Frascaria, private communication concerning: Ph.Narboni et al, Lett Nu Cim 2 (1971) 31

Gr 68 G.W. Greenlees, G.J. Pyle, Y.C. Tang, Phys Rev 171 (1968) 1115

Gr 70a G.W. Greenlees, W. Makofske, G.J. Pyle, Phys Rev C1 (1970) 1145

Gr 70b G.W. Greenlees et al, Phys Rev C2 (1970) 1063

Gr 71 G.W. Greenlees, Y.C. Tang, Phys Lett 34B (1971)359

Ha 68 S.A. Harbison et al, Nucl Phys A112 (1968) 137

Ha 70 S.A. Harbison et al, Nucl Phys A150 (1970) 570

Ha 71 H.H. Hackenbroich, P. Heiss, Z. Physik 242 (1971) 352

He 70 P. Heiss, H.H. Hackenbroich, Z. Physik 235 (1970) 422

He 72 P. Heiss, H.H. Hackenbroich, Nucl Phys A182 (1972) 522

Ho 71 P.E. Hodgson, "Nuclear Reactions and Nuclear Structure", Oxford Press 1971, 89

Hu 71 R.L. Hutson et al, Phys Rev C4 (1971) 17

Ki 64 C.C. Kim et al, Nucl Phys 58 (1964) 32

La 70 H. Langevin-Joliot et al, Nucl Phys A158 (1970) 309

Le 75 M. Le Mere, Ronald E. Brown, Y.C. Tang, to be published

Ma 74 V.A. Madsen et al, Phys Rev C9 (1974) 1253

Mc 64 D.G. McDonald et al, Phys Rev 133 (1964) B1178

Mc 70 D.H. McSherry, S.D. Baker, Phys Rev C1 (1970) 888

Mc 74 J.C.S. McKee, Laval Conference on "Few Particle Problems in the Nuclear Interaction" (1974) to be published

Mo 69 L.W. Morrow et al, Nucl Phys A126 (1969) 225

Mo 70 J.R. Morales-Pena, Thesis, Univ. of Calif. Davis (1970)

Po 74 B.S. Podmore, H.S. Sherif, Laval Conference on "Few Particle Problems in the Nuclear Interaction" (1974) to be published

Ra 74 S. Ramavataram et al, Nucl Phys A226 (1974) 173

Re 71 I. Reichstein, D.R. Thompson, Y.C. Tang, Phys Rev C3 (1971) 2139

Ro 66 L. Rosen et al, Ann Phys 34 (1966) 96

Sa 68 G.R. Satchler et al, Nucl Phys A112 (1968) 1

Sc 69 P. Schwandt, Univ of Colorado Report (1969) unpublished

Se 47 R. Serber, Phys Rev 72 (1947) 1008

Se 72 J.D. Seagrave et al, Ann Phys 74 (1972) 250

Sh pc H.S. Sherif, private communication

Sh 72 H.S. Sherif, B.S. Podmore, in "Few Particle Problems in the Nuclear Interaction" edited by I. Slaus (North-Holland, Amsterdam, 1972) 691

Ta 63 Y.C. Tang, E. Schmidt, K. Wildermuth, Phys Rev 131 (1963) 2631

Th 70 G.E. Thompson et al, Nucl Phys A142 (1970) 571

Th 73 D.R. Thompson, Y.C. Tang, J.A. Koepke, Ronald E. Brown, Nucl Phys A201 (1973) 301

Th 71 D.R. Thompson, Y.C. Tang, Phys Rev C4 (1971) 306

Ti 68 W.F. Tivol, UCRL-18137 (1968) Thesis

To 62 T.A. Tombrello et al, Nucl Phys 39 (1962) 541

To 65 T.A. Tombrello, Phys Rev 138 (1965) B40

To 66 T.A. Tombrello, Phys Rev 143 (1966) 772

Vo 68 Erich Vogt, "The Statistical Theory of Nuclear Reactions", Advances in Nuclear Physics 1 (1968) 261

Wh 37 J.A. Wheeler, Phys Rev 52 (1937) 1107

BIBILIOGRAPHY

P.E. Hodgson, "Nuclear Reactions and Nuclear Structure" Oxford 1971

Y.C. Tang, "Clustering Phenomena in Nuclei" Bochum 1969, Int. Atomic Energy Agency (1969) 109

J.A. Wheeler, Phys Rev 52 (1937) 1107

APPENDIX

ALTERNATE DERIVATION OF DIFFERENTIAL CROSS SECTION

The following derivation of the differential cross section is based on the evaporation model, as described by Vogt (Vo68). Define a wave function ψ_c, corresponding to a channel c:

$$\psi_c = r_c^{-1} \phi_\alpha \sum_{m_\ell} \sum_{m_s} (\ell s m_\ell m_s | J m_J) i^\ell Y_{\ell m_\ell} X_{s m_s} \tag{A.1}$$

where r_c is the relative separation of the pair of particles in the channel c; ϕ_α is the state of internal motion of the two particles in the channel; $i^\ell Y^\ell_{m_\ell}$ is a spherical harmonic; X_{sm_s} is the wave function of the coupled intrinsic spins l and i of the two particles, and $(\ell s m_\ell m_s | J m_J)$ is a Clebsch-Gordon coefficient.

Also, the total wave function of the system can be written:

$$\psi = \sum_c \varphi_c \psi_c \tag{A.2}$$

where φ_c are the radial wave functions for each channel. Considering only coulomb and angular momentum barriers, the radial wave equation for channel c is:

$$\left(\frac{d^2}{dr_c^2} - \frac{\ell(\ell+1)}{r_c^2} - \frac{2\eta_c k_c}{r_c} + k_c^2 \right) \varphi_c = 0 \tag{A.3}$$

where

$$\eta_c = \frac{z_1 z_2 e^2}{\hbar v_f}$$

is the usual coulomb parameter.

Equation (A.3) has the regular solution F_c and the irregular solution G_c. These solutions can be combined to give the incoming wave I_c and the outgoing wave O_c:

$$I_c = O_c^* = (G_c - iF_c)\, e^{i\omega_c} \tag{A.4}$$

where

$$\omega_c = \sum_{n=1}^{\ell_c} \tan^{-1} \frac{(\eta_c)}{n} \tag{A.5}$$

and is the coulomb phase shift. The incoing and outgoing waves have the asymptotic form:

$$I_c^* = O_c \approx \exp i(k_c r_c - \tfrac{1}{2}\ell_c\pi - \eta_c \ln 2k_c r_c) \,. \tag{A.6}$$

Since each ψ_c can be expressed as a linear combination of incoming and outgoing waves, we can write:

$$\psi = \sum_c \frac{1}{\sqrt{v_c}} (A_c I_c - B_c O_c)\psi_c \tag{A.7}$$

where A_c and B_c are amplitude coefficients and the factor $v_c^{\frac{1}{2}}$ insures unit incoming or outgoing flux. Solution of the Schrodinger equation for the whole system yields all the B_c's, i.e.:

$$B_c = \sum_{c'} U_{c\,c'} A_{c'} \tag{A.8}$$

where $U_{c\,c'}$ is the collision matrix.

Consider a nuclear reaction which has an initial pair of particles α and a final pair of particles α' observed in a direction (θ, φ) relative to the incident beam. The total wave function can be written:

$$\psi = \psi_{inc} + \psi_{reac} \tag{A.9}$$

where ψ_{inc} is the incident plane wave and

$$\psi_{inc} = \phi_\alpha \chi_{sm_s} \exp(ik_\alpha z_\alpha)$$

$$= \phi_\alpha \chi_{sm_s} \sqrt{4\pi} \sum_{\ell=0}^{\infty} (2\ell+1)^{\frac{1}{2}} j_\ell(k_\alpha r_\alpha) i^\ell Y_\ell^0(\theta, \varphi) \; . \tag{A.10}$$

In order to obtain the A_c's, Equation (A.10) is compared with the incoming and outgoing waves at distances where the coulomb fields of the target and projectile are screened from each other. This gives us:

$$j_\ell(k_\alpha r_\alpha) \simeq \frac{F_\ell(k_\alpha r_\alpha)}{k_\alpha r_\alpha} = \frac{i(I_\ell - O_\ell)}{2k_\alpha r_\alpha} \; . \tag{A.11}$$

Substituting Equation (A.11) into Equation (A.10), we obtain:

$$\psi_{inc} = \phi_\alpha \sum_{J=0}^{\infty} \sum_{m_J=-J}^{J} \sum_{\ell=|J-s|}^{J+s} ik_\alpha^{-1} \pi^{\frac{1}{2}} (\ell s 0 m_s | J m_J)(2\ell+1)^{\frac{1}{2}} r_\alpha^{-1}$$

$$\times \sum_{m_\ell=-\ell}^{\ell} \sum_{m_s=-s}^{s} (\ell s m_\ell m_s | J m_J)(I_\ell - O_\ell) Y_\ell^0 \chi_{sm_s} \; . \tag{A.12}$$

Therefore,

$$A_c \equiv A_c \equiv A_{\alpha s \ell}^{Jm_J} = ik_\alpha^{-1} (\pi v_\alpha)^{\frac{1}{2}} (\ell s 0 m_s | J m_J)(2\ell+1)^{\frac{1}{2}} \tag{A.13}$$

for the α, s, and m_s of the incident beam; $A_c = 0$ for all other channels. Also,

$$B_{c'} \equiv B_{\alpha' s' \ell'}^{Jm_J} = i(k_c)^{-1} (\pi v_c)^{\frac{1}{2}} \sum_{\ell=|J-s|}^{J+s} (\ell s 0 m_s | J m_J)(2\ell+1)^{\frac{1}{2}} U_{\alpha s \ell ; \alpha' s' \ell'}^{J} \; . \tag{A.14}$$

Using Equations (A.9), (A.12) and (A.14), we can write:

$$\psi_{reac} = \sum_{c} \sum_{c'} (\delta_{cc'} - U_{cc'}) A_{c'} O_{c'} \quad . \tag{A.15}$$

The kronecker delta accounts for outgoing waves in the incident plane wave. A more useful form for ψ_{reac} is in terms of the laboratory variables:

$$\psi_{reac} \equiv i \sum_{\alpha', s', m_{s'}} k_{\alpha}^{-1} (v_{\alpha}/v_{\alpha'})^{\frac{1}{2}} r_{\alpha'}^{-1} e^{ik_{\alpha'} r_{\alpha'}} \phi_{\alpha'} \chi_{s'm_{s'}} \times q_{\alpha's'm_{s'};\alpha s m_s}(\theta, \varphi) \tag{A.16}$$

where

$$q_{\alpha's'm_{s'};\alpha s m_s}(\theta, \varphi) = -\sum_{J=0}^{\infty} \sum_{m_J=-J}^{J} \sum_{\ell=|J-s|}^{J+s} \sum_{\ell'=|J-s'|}^{J+s'} \sum_{m_{\ell'}=-\ell'}^{\ell'} \times \pi^{\frac{1}{2}} (2\ell+1)^{\frac{1}{2}} (\ell s 0 m_s | J m_J) (\ell' s' m_{\ell'}, m_{s'} | J m_J) \times (\delta_{\alpha\alpha'} \delta_{ss'} \delta_{\ell\ell'} - U^{J}_{\alpha's'\ell';\alpha s\ell}) i^{\ell'} Y_{\ell' m_{s'}}(\theta, \varphi) \quad . \tag{A.17}$$

Now, the differential cross section for the reaction $\alpha \rightarrow \alpha'$ can be written:

$$\frac{d\sigma_{\alpha\alpha'}}{d\Omega} = k_{\alpha}^{-2} \sum_{m_s=-s}^{s} \sum_{m_{s'}=-s'}^{s'} \sum_{s=|I-i|}^{I+i} \sum_{s'=|I'-i'|}^{I'+i'} \frac{1}{(2\ell+1)(2i+1)} \times |q_{\alpha's'm_{s'};\alpha s m_s}(\theta, \varphi)|^2 \quad . \tag{A.18}$$

This equation can be simplified by performing some of the sums over the Clebsch-Gordon coefficients, to obtain:

$$\frac{d\sigma_{\alpha\alpha'}}{d\Omega} = \frac{1}{k_\alpha^2} \sum_{L=0}^{\infty} B_L(\alpha,\alpha') P_L(\cos\theta) \qquad (A.19)$$

where

$$B_L(\alpha,\alpha') = \sum_{m_s,m_s',s,s',J_1,J_2,\ell_1,\ell_2,\ell_1',\ell_2'} \frac{(-)^{s-s'}}{4(2I+1)(2i+1)}$$

$$\times i^{\ell_1-\ell_2-L} Z(\ell_1 J_1 \ell_2 J_2; sL) i^{\ell_1'-\ell_2'-L} Z(\ell_1' J_1 \ell_2' J_2; sL)$$

$$\times RP[(\delta_{\alpha\alpha'}\delta_{\ell_1\ell_1'}\delta_{ss'} - U^{J_1}_{\alpha's'\ell_1';\alpha s\ell_1})^*$$

$$\times (\delta_{\alpha\alpha'}\delta_{ss'}\delta_{\ell_2\ell_2'} - U^{J_2}_{\alpha's'\ell_2';\alpha s\ell_2})] \qquad (A.20)$$

where Z's are the Z coefficients defined by Biedenharn, Blatt and Rose (Bi52)

$$Z(abcd;ef) = i^{f+a+c}[(2a+1)(2b+1)(2c+1)(2d+1)]^{\frac{1}{2}} W(abcd;ef)(ac00|acf0)$$

where W is a Racah coefficient, and

$$(ac00|acf0) = \begin{cases} (-1)^{g+f}\sqrt{2f+1}\,\Delta(acf)\,\dfrac{g!}{(g-a)!(g-c)!(g-f)!} & \text{for } a+b+c \text{ even} \\ 0 & \text{for } a+b+c \text{ odd} \end{cases}$$

where $g = \frac{1}{2}(a+c+f)$

and $\Delta(acf) = \left[\dfrac{(a+c-f)!(a-c+f)!(-a+c+f)!}{(a+c+f+1)!}\right]^{\frac{1}{2}}$

For elastic scattering:

$$\frac{d\sigma_{\alpha\alpha}}{d\Omega} = \frac{1}{k_\alpha^2} \sum_{L=0}^{\infty} B_L(\alpha,\alpha) P_L(\cos\theta) \qquad (A.21)$$

where

$$B_L(\alpha,\alpha) = \sum_{\substack{m_s,s,J_1,J_2 \\ \ell_1,\ell_2}} \frac{(-)^{\ell_1-\ell_2-L}}{4(2I+1)(2i+1)} [Z(\ell_1 J_1 \ell_2 J_2; sL)]^2 \times \text{Real Part}[(1-U^{J_1}_{\alpha s\ell_1;\alpha s\ell_1})^*(1-U^{J_2}_{\alpha s\ell_2;\alpha s\ell_2})] \ . \qquad (A.22)$$

Tombrello obtained an equation for the differential cross section for spin-1/2 - spin-1/2 scattering in the center of mass system (To62):

$$\sigma(\theta) = \frac{1}{2k^2} (|a|^2 + |b|^2 + |c|^2 + |d|^2 + |e|^2 + |f|^2 + |g|^2 + |h|^2) \ , \qquad (A.23)$$

where

$$a = \tfrac{1}{2} i\eta \csc^2 \tfrac{1}{2}\theta \, e^{i\eta \ln \csc^2 \frac{1}{2}\theta} + \sum_{\ell=0}^{\infty} \tfrac{1}{4} P_\ell(\cos\theta) \{ -\sqrt{\ell(\ell-1)} U^{\ell-1}_{(\ell,1;\ell-2,1)} + (\ell+2) U^{\ell+1}_{(\ell,1;\ell,1)} + (2\ell+1) U^{\ell}_{(\ell,1;\ell,1)} + (\ell-1) U^{\ell-1}_{(\ell,1;\ell,1)} - \sqrt{(\ell+1)(\ell+2)}\, U^{\ell+1}_{(\ell,1;\ell+2,1)} \} \ ,$$

$$b = \tfrac{1}{2} i\eta \csc^2 \tfrac{1}{2}\theta \, e^{i\eta \ln \csc^2 \frac{1}{2}\theta} + \sum_{\ell=0}^{\infty} \tfrac{1}{4} P_\ell(\cos\theta) \sqrt{\ell(\ell-1)}\, U^{\ell-1}_{(\ell,1;\ell-2,1)} + (\ell+1) U^{\ell+1}_{(\ell,1;\ell,1)} + \ell U^{\ell-1}_{(\ell,1;\ell,1)} + \sqrt{(\ell+1)(\ell+2)}\, U^{\ell+1}_{(\ell,1;\ell+2,1)} + (2\ell+1) U^{\ell}_{(\ell,0,\ell,0)} \} \ ,$$

$$c = \sum_{\ell=0}^{\infty} \frac{1}{4} P_\ell(\cos\theta)\{\sqrt{\ell(\ell-1)}U^{\ell-1}_{(\ell,1;\ell-2,1)} + (\ell+1)U^{\ell+1}_{(\ell,1;\ell,1)}$$

$$+ \ell U^{\ell-1}_{(\ell,1;\ell,1)} + \sqrt{(\ell+1)(\ell+2)}U^{\ell+1}_{(\ell,1;\ell+2,1)} - (2\ell+1)U^{\ell}_{(\ell,0;\ell,0)}\} ,$$

$$d = \sum_{\ell=1}^{\infty} -\frac{1}{4} i \sin\theta \frac{P'_\ell(\cos\theta)}{\sqrt{\ell(\ell+1)}} \{-\sqrt{(\ell-1)(\ell+1)}U^{\ell-1}_{(\ell,1;\ell-2,1)} + \sqrt{\ell(\ell+1)}U^{\ell+1}_{(\ell,1;\ell,1)}$$

$$- \sqrt{\ell(\ell+1)}U^{\ell-1}_{(\ell,1;\ell,1)} + \sqrt{\ell(\ell+2)}U^{\ell+1}_{(\ell,1;\ell+2,1)} - (2\ell+1)U^{\ell}_{(\ell,1;\ell,0)}\} ,$$

$$e = \sum_{\ell=1}^{\infty} -\frac{1}{4} i \sin\theta \frac{P'_\ell(\cos\theta)}{\sqrt{\ell(\ell+1)}} \{-\sqrt{(\ell-1)(\ell+1)}U^{\ell-1}_{(\ell,1;\ell-2,1)} + \sqrt{\ell(\ell+1)}U^{\ell+1}_{(\ell,1;\ell,1)}$$

$$- \sqrt{\ell(\ell+1)}U^{\ell-1}_{(\ell,1;\ell,1)} + \sqrt{\ell(\ell+2)}U^{\ell+1}_{(\ell,1;\ell+2,1)} + (2\ell+1)U^{\ell}_{(\ell,1;\ell,0)}\} ,$$

$$f = \sum_{\ell=2}^{\infty} -\frac{1}{4} \sin^2\theta \frac{P''_\ell(\cos\theta)}{\sqrt{(\ell-1)\ell(\ell+1)(\ell+2)}} \left\{- \sqrt{(\ell+1)(\ell+2)}U^{\ell-1}_{(\ell,1;\ell-2,1)}\right.$$

$$+ \sqrt{\frac{\ell(\ell-1)(\ell+2)}{\ell+1}}\, U^{\ell+1}_{(\ell,1;\ell,1)} - (2\ell+1)\sqrt{\frac{(\ell-1)(\ell+2)}{\ell(\ell+1)}}\, U^{\ell}_{(\ell,1;\ell,1)}$$

$$\left. + \sqrt{\frac{(\ell-1)(\ell+1)(\ell+2)}{\ell}}\, U^{\ell-1}_{(\ell,1;\ell,1)} - \sqrt{\ell(\ell-1)}U^{\ell+1}_{(\ell,1;\ell+2,1)}\right\} ,$$

$$g = \sum_{\ell=1}^{\infty} -\frac{1}{4} i \sin\theta \frac{P'_\ell(\cos\theta)}{\sqrt{\ell(\ell+1)}} \left\{\sqrt{(\ell-1)(\ell+1)}U^{\ell-1}_{(\ell,1;\ell-2,1)} + (\ell+2)\sqrt{\frac{\ell}{\ell+1}}\, U^{\ell+1}_{(\ell,1;\ell,1)}\right.$$

$$- \frac{(2\ell+1)}{\sqrt{\ell(\ell+1)}}\, U^{\ell}_{(\ell,1;\ell,1)} - (\ell-1)\sqrt{\frac{\ell+1}{\ell}}\, U^{\ell-1}_{(\ell,1;\ell,1)}$$

$$\left. - \sqrt{\ell(\ell+2)}U^{\ell+1}_{(\ell,1;\ell+2,1)} - (2\ell+1)U^{\ell}_{(\ell,0;\ell,1)}\right\} ,$$

$$h = \sum_{\ell=1}^{\infty} -\frac{1}{4} i \sin\theta \frac{P'_\ell(\cos\theta)}{\sqrt{\ell(\ell+1)}} \left\{ \sqrt{(\ell-1)(\ell+1)}\, U^{\ell-1}_{(\ell,1;\ell-2,1)} + (\ell+2)\sqrt{\frac{\ell}{\ell+1}}\, U^{\ell+1}_{(\ell,1;\ell,1)} \right.$$

$$- \frac{(2\ell+1)}{\sqrt{\ell(\ell+1)}} U^{\ell}_{(\ell,1;\ell,1)} - (\ell-1)\sqrt{\frac{\ell+1}{\ell}}\, U^{\ell-1}_{(\ell,1;\ell,1)}$$

$$\left. - \sqrt{\ell(\ell+2)}\, U^{\ell+1}_{(\ell,1;\ell+2,1)} + (2\ell+1) U^{\ell}_{(\ell,0;\ell,1)} \right\} ,$$

$$U^{j}_{(\ell',s';\ell,s)} = e^{i(\alpha_\ell + \alpha_{\ell'})} (\delta_{\ell,\ell'}\delta_{s,s'} - S^{j}_{(\ell',s';\ell,s)}) = U^{j}_{(\ell,s;\ell',s')} ,$$

where $S^{j}_{(\ell',s';\ell,s)}$ is the element of the scattering matrix for total angular momentum j connecting initial orbital angular momentum ℓ' and channel spin s', with their final values ℓ and s. In these formulae

$$\eta = \frac{Z_1 Z_2 e^2}{\hbar v} , \qquad k = \frac{\mu v}{\hbar} , \qquad \alpha_0 = 0 , \qquad \alpha_\ell = \sum_{s=1}^{\ell} \text{arctg}(\eta/s) ,$$

where v is the relative velocity of the two particles, and μ is the reduced mass of the system .

The polarization of the scattered protons (To65) is given by

$$P_p(\theta) = -\left(\frac{2\,\text{Re}(ae^* + bh^* + cg^* + df^*)}{|a|^2+|b|^2+|c|^2+|d|^2+|e|^2+|f|^2+|g|^2+|h|^2} \right) (\hat{k}_{in} \times \hat{k}_{out})$$

and the polarization of the recoil He^3's is

$$P_{He^3} = -\left(\frac{2\,\text{Re}(ad^* + bg^* + ch^* + ef^*)}{|a|^2+|b|^2+|c|^2+|d|^2+|e|^2+|f|^2+|g|^2+|h|^2} \right) (\hat{k}_{in} \times \hat{k}_{out}) . \qquad \text{(A.24)}$$

Note that in Equation (A.23) the $U^{J}_{\alpha's'\ell';\ell s}$'s are written as $U^{J}_{(s'\ell';s\ell)}$.